Supporting Information

Ultra-small Zr-MOF nanoparticles as heterogeneous catalysts for direct amide bond formations

Isabel Abanadés Lázaro[a]*, Ross S. Forgan[b] and Francisco. G. Cirujano[a]*

[a] Instituto de Ciencia Molecular (ICMol), Universitat de Valencia, Catedrático José Beltrán Martínez nº 2, 46980 Paterna, Valencia, Spain

[b] WestCHEM School of Chemistry, University of Glasgow, Joseph Black Building, University Avenue, Glasgow G12 8QQ, UK
*Correspondence: isabel.abanades@uv.es; francisco.c.garcia@uv.es

Table of Contents

S1. General Experimental Remarks

Powder X-Ray Diffraction (PXRD): PXRD patterns were collected in a PANalyticalX'Pert PRO diffractometer using copper radiation (Cu Kα = 1.5418 Å) with an X'Celerator detector, operating at 40 mA and 45 kV. Profiles were collected in the 3° < 2θ < 40° range with a step size of 0.017°. (University of Valencia)

Thermogravimetric Analysis (TGA): were carried out with a Mettler Toledo TGA/SDTA 851 apparatus between 25 and 800 °C under ambient conditions (10 °C·min^{-1} scan rate and an air flow of 9 mL·min−1). (University of Valencia)

Nuclear Magnetic Resonance Spectroscopy (NMR): NMR spectra were recorded on either a Bruker AVIII 300 MHz spectrometer and referenced to residual solvent peaks. (University of Valencia)

Gas Uptake: N_2 adsorption isotherms were carried out at 77 K on a Quantachrome Autosorb iQ gas sorption analyser. Samples were degassed under vacuum at 120 °C for 20 hours using the internal turbo pump. BET surface areas were calculated from the isotherms using the Micropore BET Assistant in the Quantachrome ASiQwin operating software. (University of Glasgow)

Scanning Electron Microscopy (SEM) and single point energy-dispersive X-Ray analysis (EDX): particle morphologies, dimensions and mapping were studied with a Hitachi S-4800 scanning electron microscope at an accelerating voltage of 20 kV. No coating was performed. Particle size distribution was analysed manually using ImageJ software and calculated from a minimum of 50 nanoparticles. (University of Valencia)

Fourier Transform Infrared Spectroscopy: IR spectra of solids were collected using a Shimadzu Fourier Transform Infrared Spectrometer, FTIR-8400S, fitted with a Diamond ATR unit. (University of Valencia)

For the quantification of the reaction yield, we have focused on the following H-NMR spectroscopic signals of reagents and products. Aniline ^{1}H NMR (300 MHz, DMSO-d_6) δ 7.06 – 6.98 (m, 2H), 6.66 – 6.48 (m, 3H). Formanilidine ^{1}H NMR (300 MHz, DMSO) δ 8.26 (t, J = 2.1 Hz, 1H), 7.58 (dt, J = 8.7, 1.7 Hz, 2H), 7.35 – 7.26 (m, 3H). In the case of *N*-benzyl-2-phenylacetamide, the signal at ca. 3.6 (s, 2H) was used to quantify the yield, based on the remaining reagent characterized by the signal at ca. 3.5 (s, 2H).

S.2. Materials and Synthesis

All reagents unless otherwise stated were obtained from commercial sources and were used without further purification.

Synthesis of ultra-small particles: In separate vials, zirconyl chloride octahydrate (213 mg, 0.66 mmol, 1 equivalent) and the linker (1.65 mmol, 2.5 equivalents) were dissolved in 20 mL of DMF. After mixing both precursor solutions in 80 mL mL pyrex jars, acetic acid (12 mmol, 18.2 equivalents) was added to the reaction mixture which, after gently stirring, was placed in the oven at 120 °C for 24 h. After cooling to room temperature, the powders were collected by centrifugation, and washed with DMF (X2) and MeOH (X3) through dispersion centrifugation cycles. The resultant NMOFs were dried under vacuum for at least 24 hours prior to analysis.

Synthesis of standard Zr-BDC-NH_2: 2-aminoterephthalic acid (bdc- NH_2) (122 mg, 0.675 mmol) was dissolved in 7.5 mL of DMF, and 0.9 mL of acetic acid (6% volume) was added to the solution. In a separate vial, the metal precursor, zirconium chloride (157 mg, 0.675 mmol) was dissolved in 7.5 mL of DMF. The solutions were mixed together in a 25 mL jar, which was placed in an oven and heated to 120 ºC for 24 hours.

^{1}H NMR characterization: approximately 5 mg of MOF were digested in 0.6 mL of DMSO-d_6 with 5 drops of D_2SO_4 by heating at 75°C and stirring until complete dissolution.

Activation: The precipitate was collected by centrifugation and washed with DMF (X2) and MeOH (X3)

Catalytic test: Product A: 100 µL of aniline (1.1 mmol) and 200 µL of formic acid (5.3 mmol) were added to a glass vial containing 10 mg of MOF and the mixture was heating at 35 ºC under stirring at 300 rpm. Sample aliquots were taken at different times, diluted with DMSO-d_6 and analyzed by ^{1}H-NMR spectroscopy. The larger peak areas corresponding to the three protons of the aromatic ring of the aniline reagent and formamidine product were employed for the calculation of the yield, in order to minimize the error. Product B: 20 mg of phenyl acetic acid (0.15 mmol) and 20 µL of benzylamine (0.19 mmol) were dissolved in 200 µL of CD_3OD and added to a vial containing 10 mg of MOF. The mixture was heated at 60 ºC for 24 h. Sample aliquots were taken at different times, diluted with CD_3OD and analyzed by ^{1}H-NMR spectroscopy.

Catalyst recyclability: For the recycling test, the spent MOF was thoroughly washed with ethanol and acetone and recovered by centrifugation. The dry MOF sample (30 mg MOF Zr-BDC-NH_2) was tested in two subsequent reaction cycles between 200 µL aniline and 400 µL formic, 35 ºC during a reaction time of 30 min.

S.3. Characterisation

S.3.1. PXRD patterns

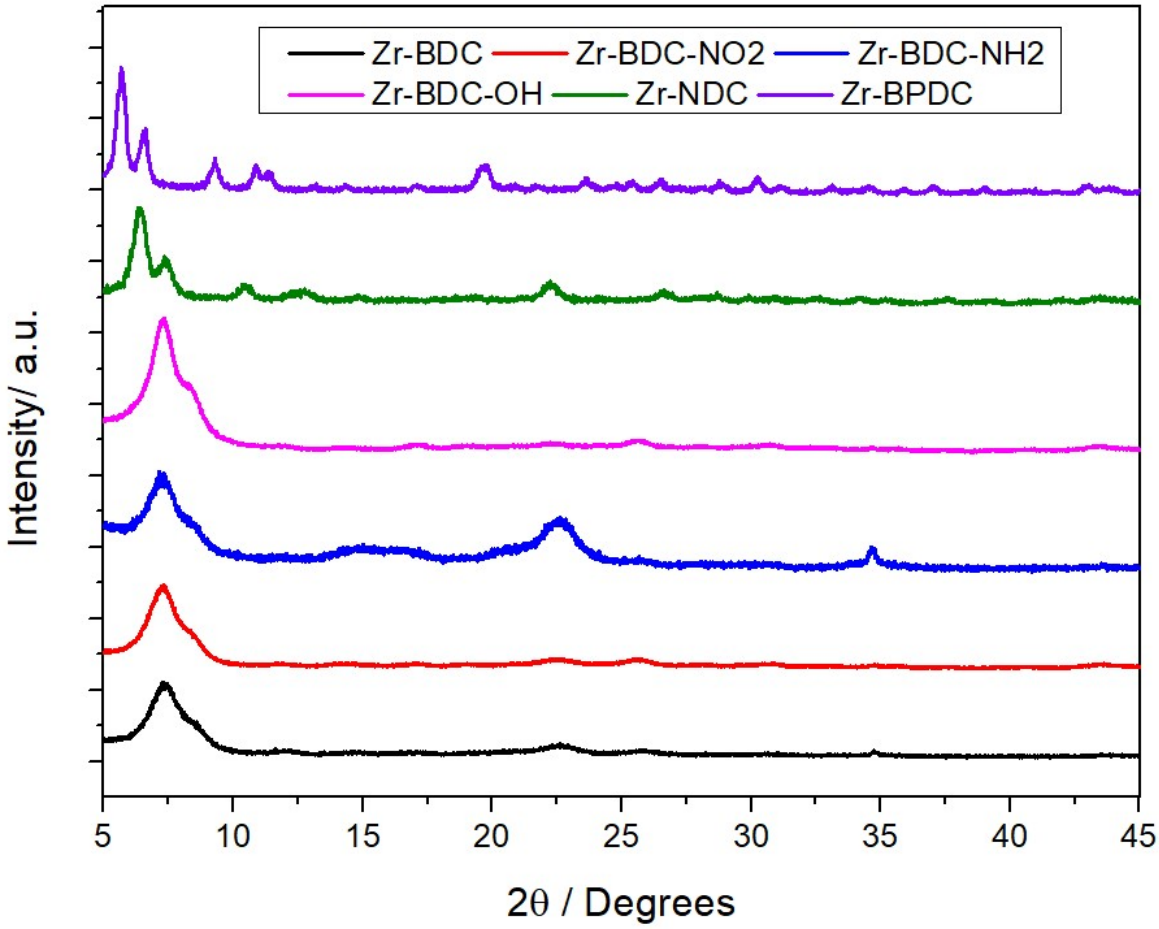

Figure S1: PXRD patterns of ultra-small Zr MOFs synthesized with different linkers, showing the UiO **fcu** topology.

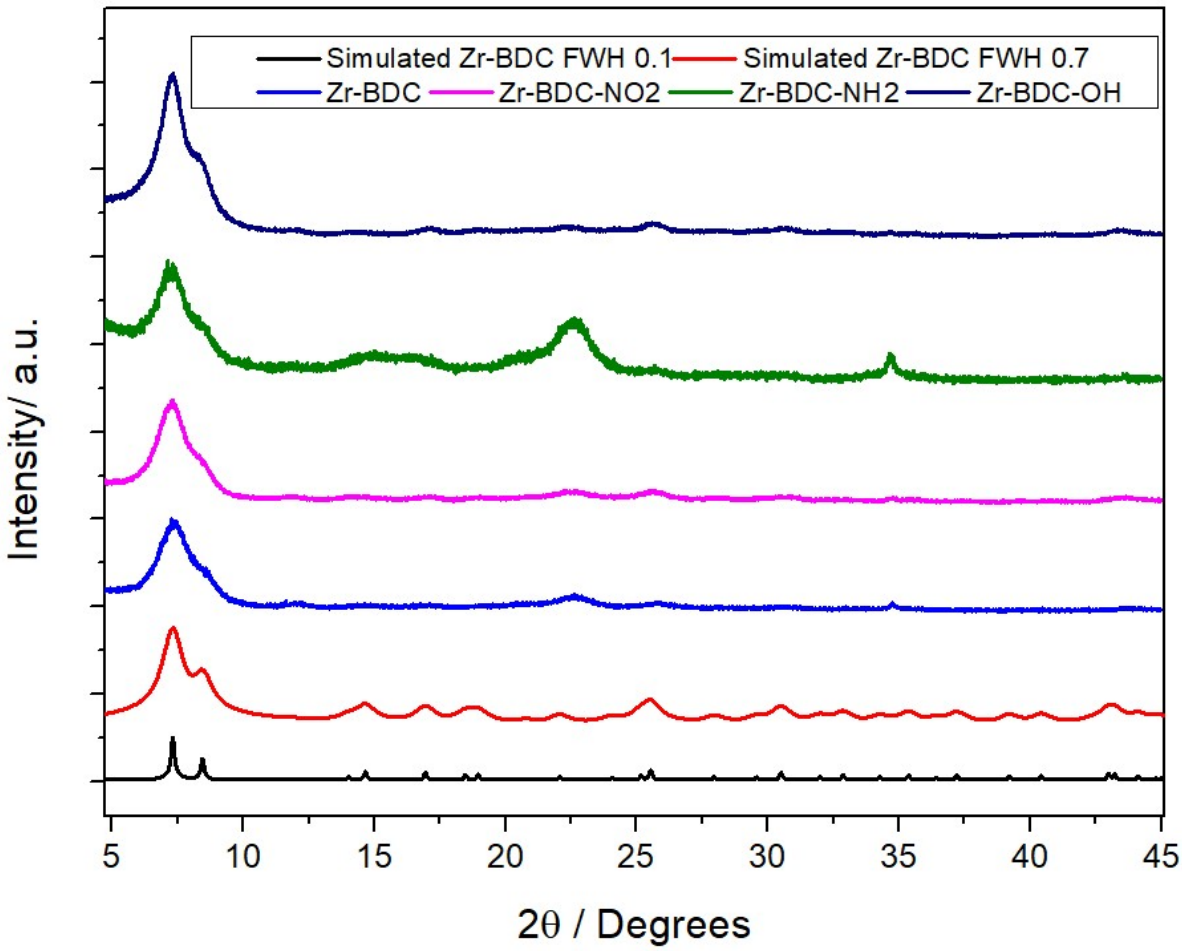

Figure S2: PXRD patterns of ultra-small Zr MOFs synthesized with BDC linkers compared with the simulated patterns with different Bragg reflection bands width. The wider Bragg reflections are a consequence of the small particle size of the samples, and as shown by the comparison with simulated patterns, the resolution of the spectra decreases with the peak width.

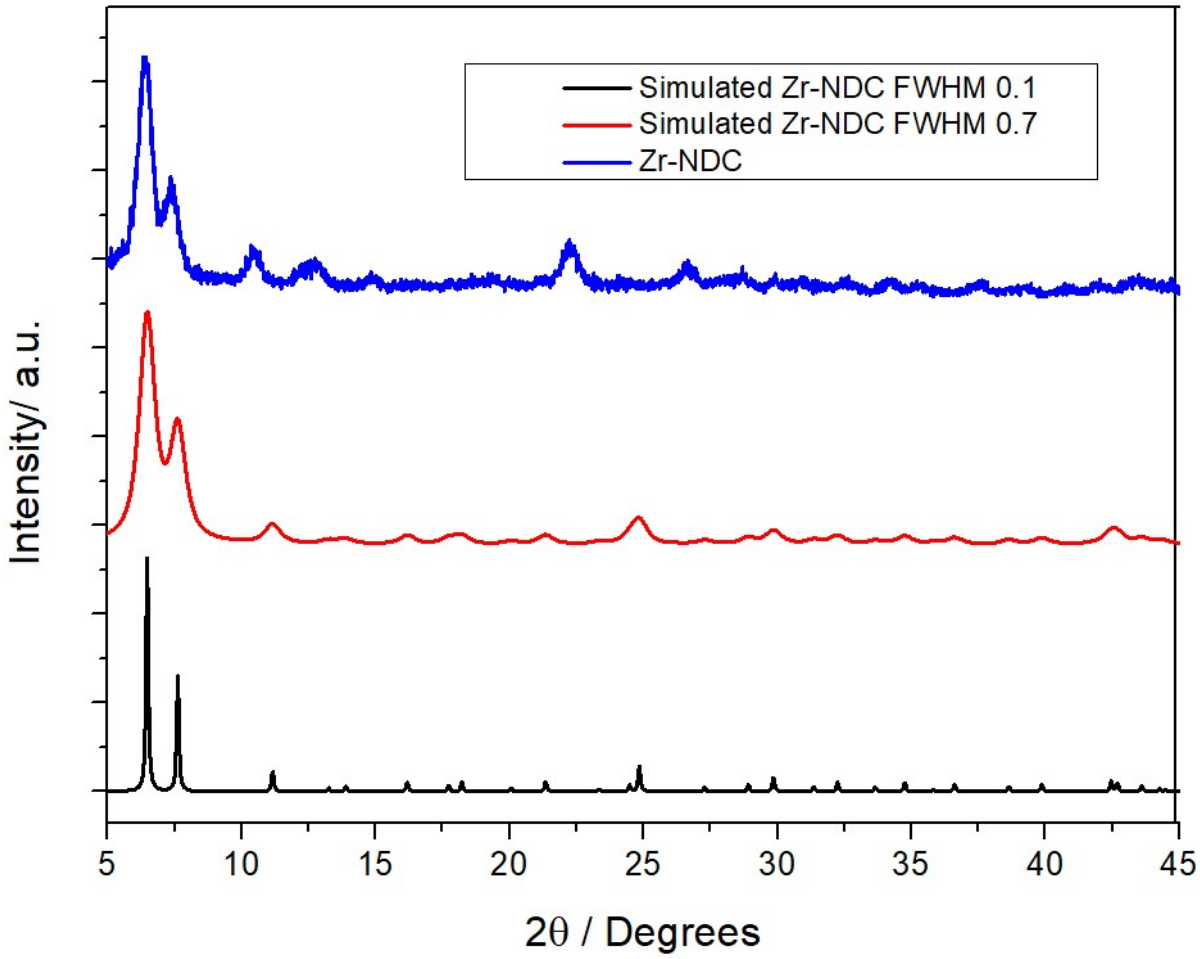

Figure S3: PXRD patterns of the ultra-small Zr-NDC MOF compared with the simulated patterns with different Bragg reflection bands width. The wider Bragg reflections are a consequence of the small particle size of the samples, and as shown by the comparison with simulated patterns, the resolution of the spectra decreases with the peak width.

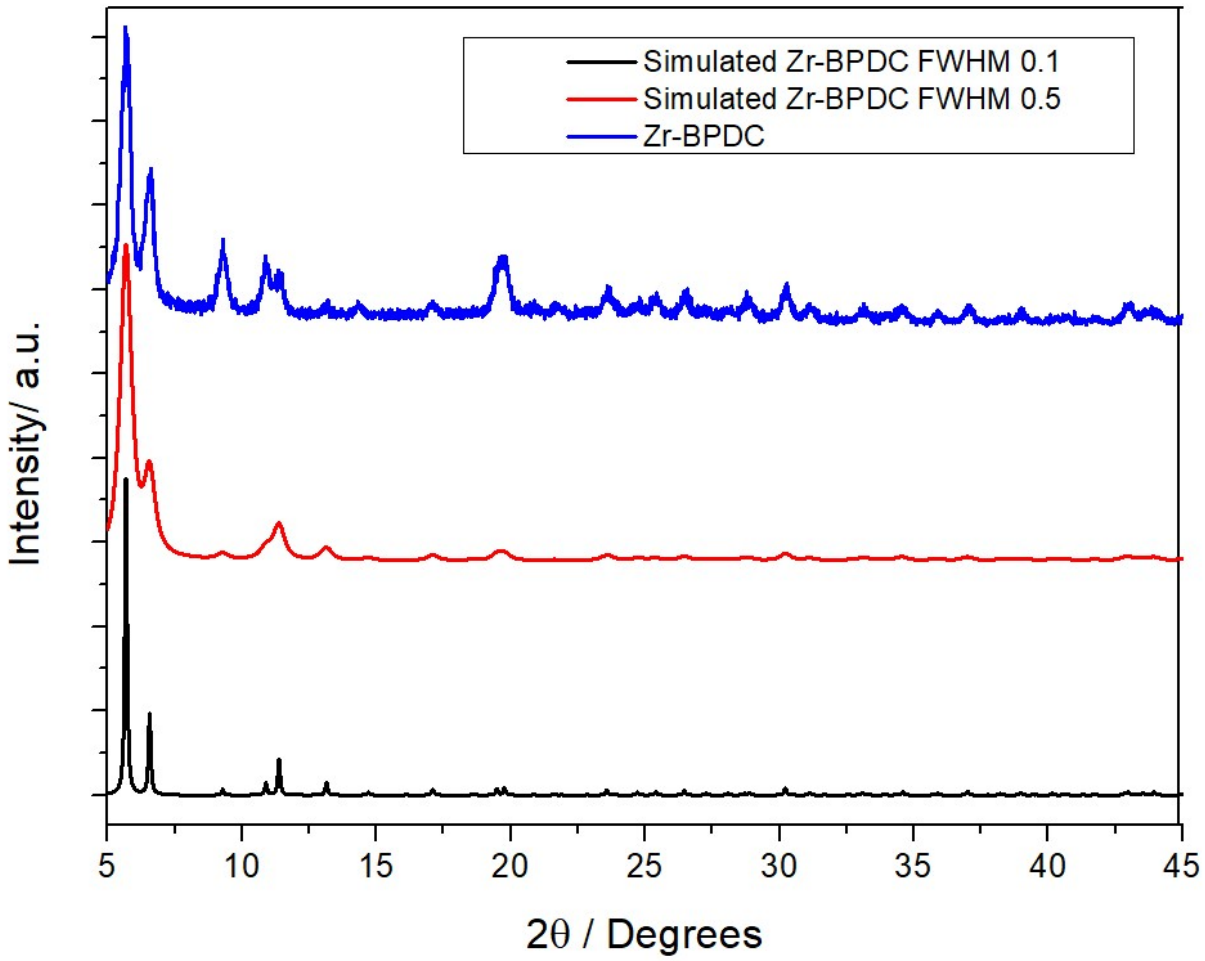

Figure S4: PXRD patterns of the ultra-small Zr-BPDC MOF compared with the simulated patterns with different Bragg reflection bands width. The wider Bragg reflections are a consequence of the small particle size of the samples, and as shown by the comparison with simulated patterns, the resolution of the spectra decreases with the peak width.

S.3.2. Particle size

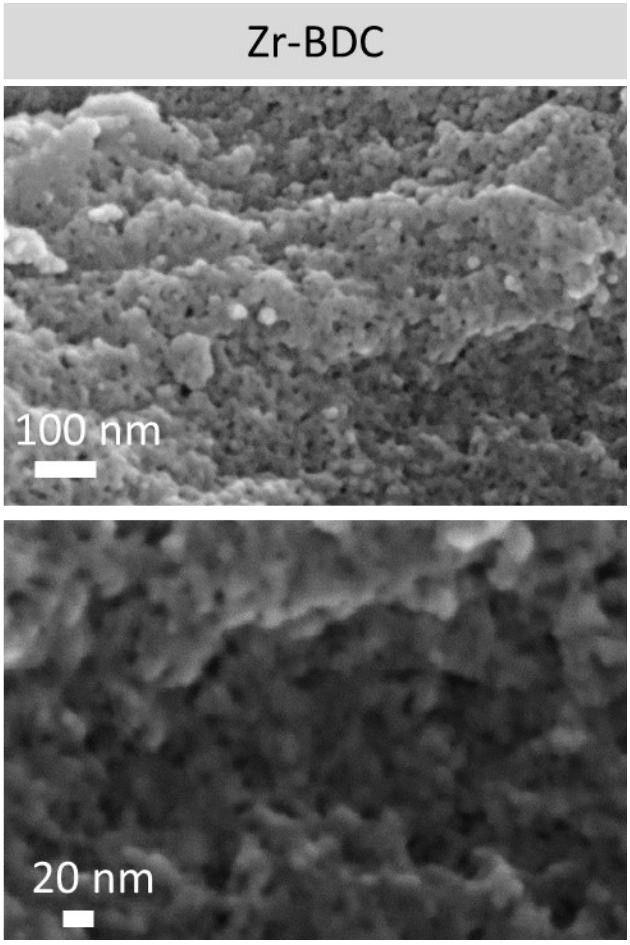

Figure S5: SEM images of ultra-small Zr-BDC.

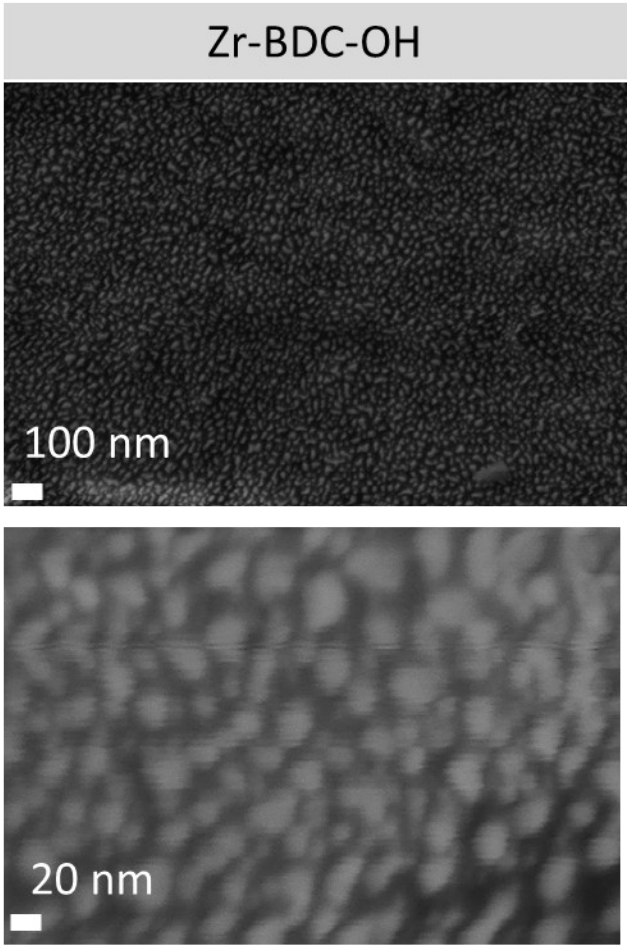

Figure S6: SEM images of ultra-small Zr-BDC-OH.

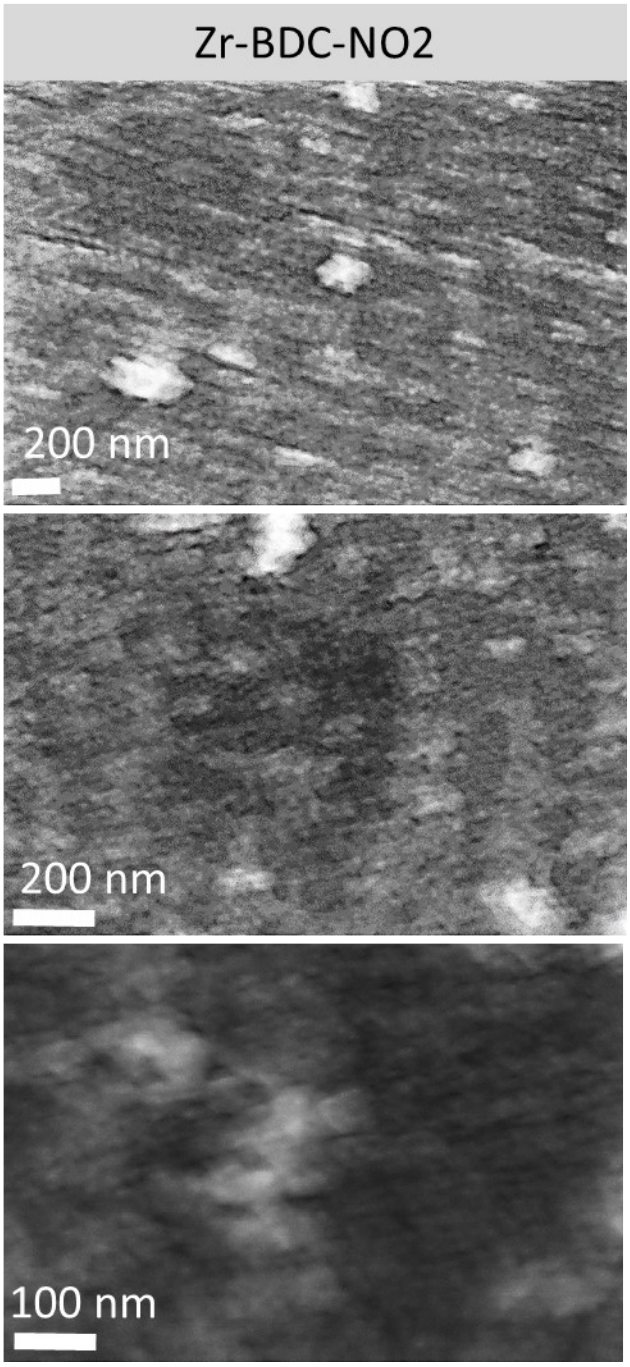

Figure S7: SEM images of ultra-small Zr-BDC-NO_2.

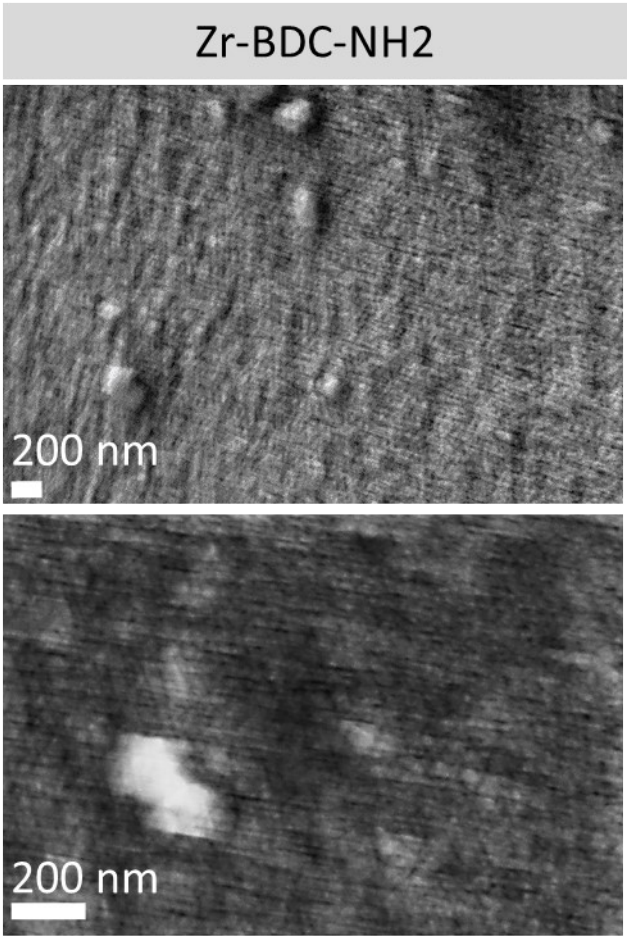

Figure S8: SEM images of ultra-small Zr-BDC-NH_2.

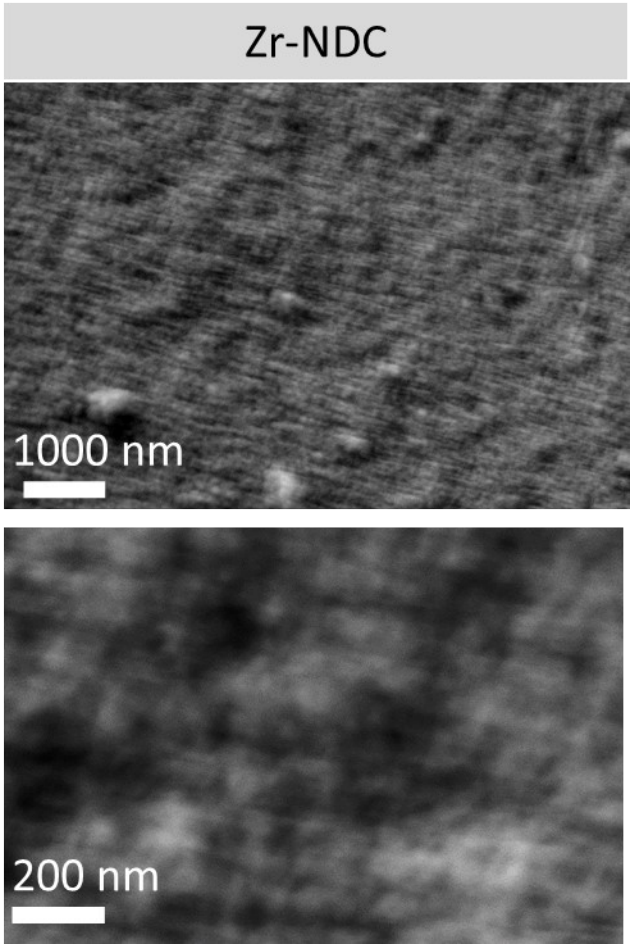

Figure S9: SEM images of ultra-small Zr-NDC.

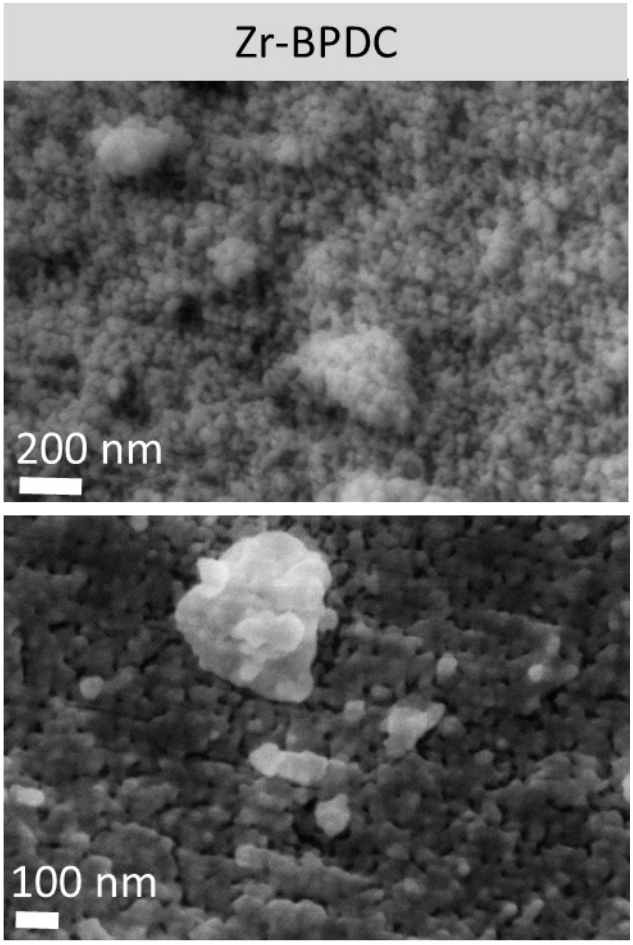

Figure S10: SEM images of ultra-small Zr-BPDC.

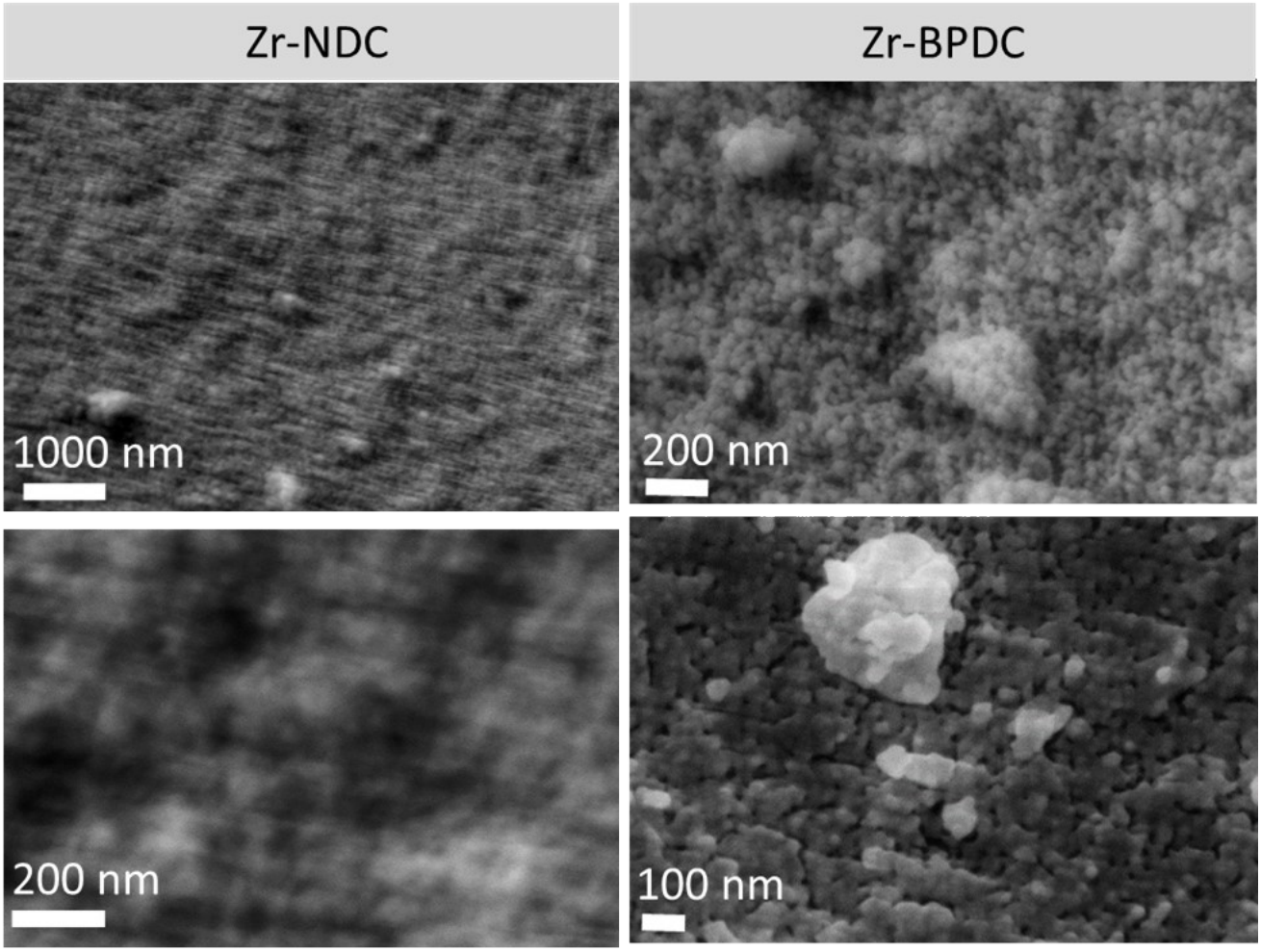

Figure S11: SEM images of ultra-small Zr- MOFs with extended linkers.

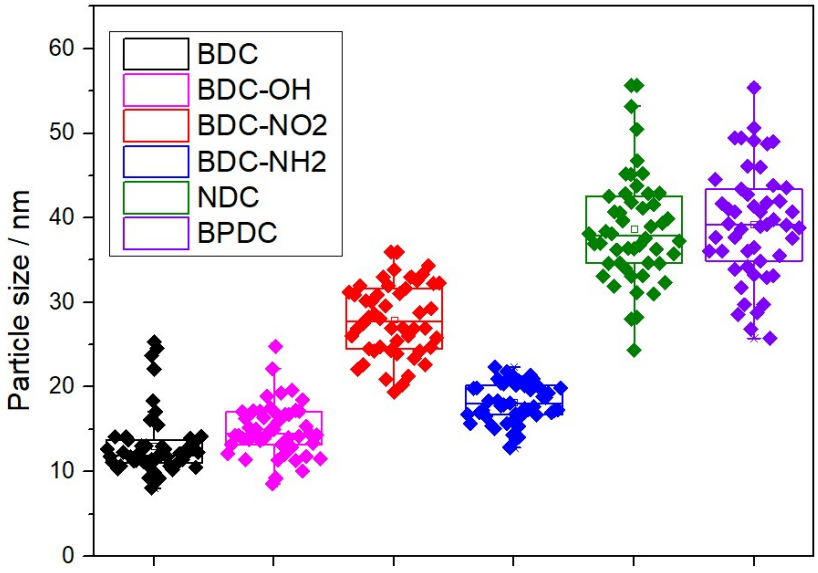

Figure S12: Box chart representation of ultra-small Zr-MOFs particle sizes. Bin size of 5 nm. Average size and standard deviation, 25% and 75% quartiles.

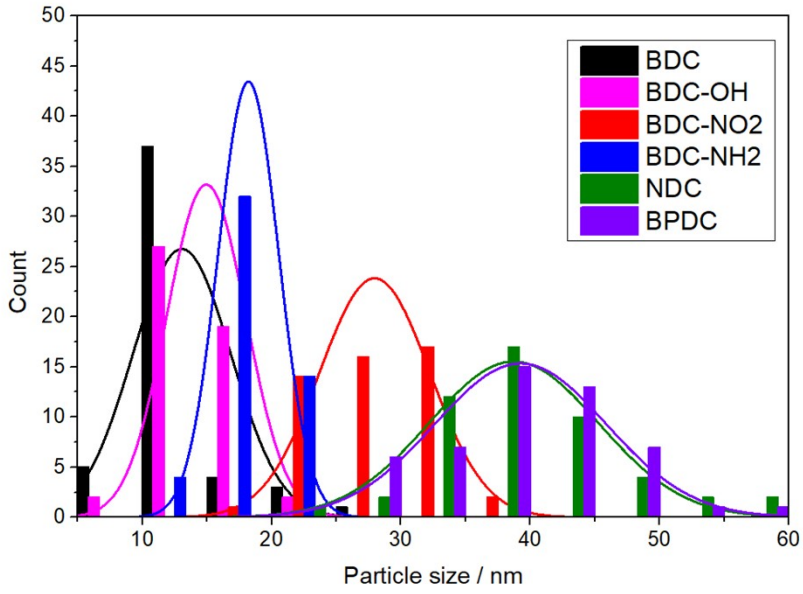

Figure S13: Histograms of ultra-small Zr-MOFs particle sizes together with particle size distribution curve. Bin size of 5 nm.

Table S1: Tabulated particle sizes and standard deviations of ultra-small Zr-MOFs. Units are given in nanometers.

SAMPLE	Zr-BDC	Zr-BDC-OH	Zr-BDC-NO_2	Zr-BDC-NH_2	Zr-NDC	Zr-BPDC
Average particle size	13.04	14.94	27.96	18.19	38.72	39.25
Standard deviation	3.76	3.03	4.22	2.31	6.48	6.56

3.3. Dynamic Light Adsorption measurements

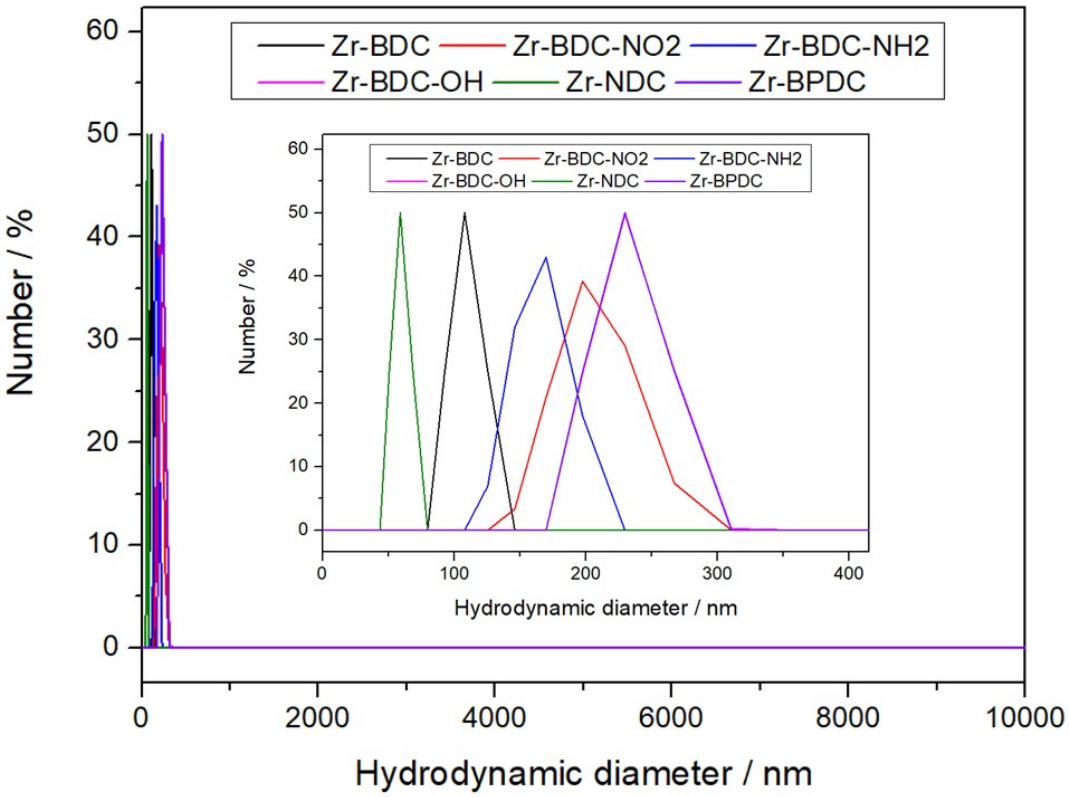

Figure S14: Hydrodynamic diameter determined by Dynamic Light Scattering measurements of *ca.* 0.1 mg mL^{-1} dispersions in MeOH.

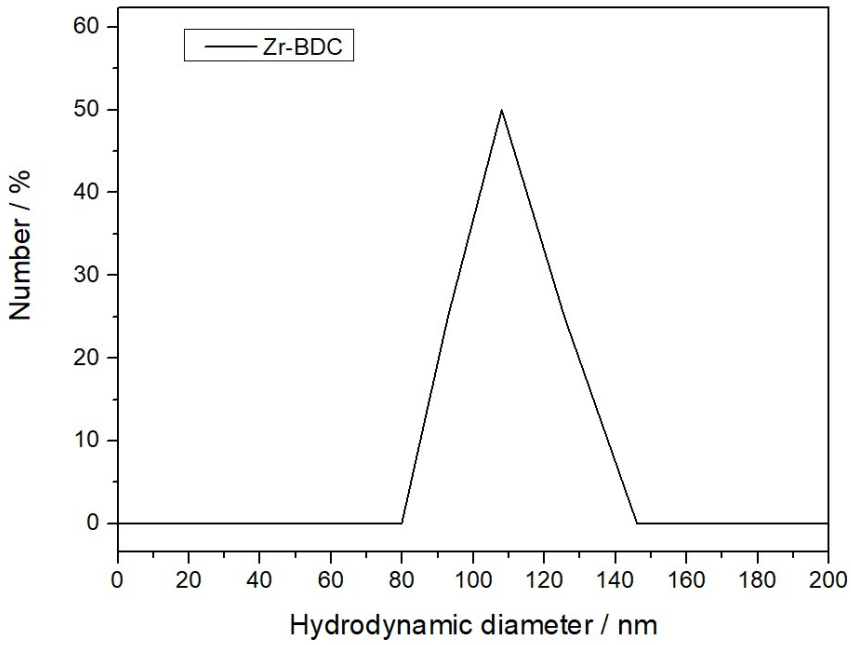

Figure S15: Hydrodynamic diameter of Zr-BDC determined by Dynamic Light Scattering measurements of *ca.* 0.1 mg mL^{-1} dispersions in MeOH.

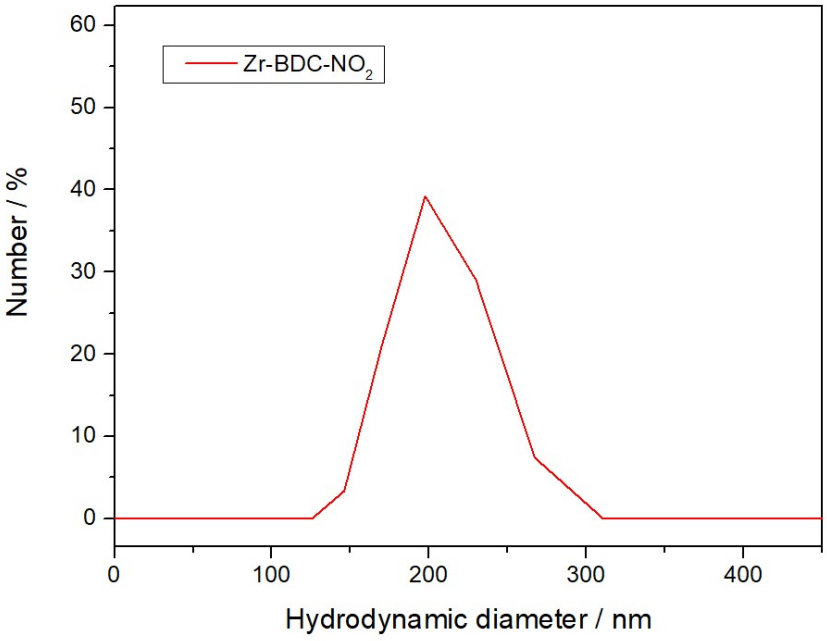

Figure S16: Hydrodynamic diameter of Zr-BDC-NO_2 determined by Dynamic Light Scattering measurements of *ca.* 0.1 mg mL^{-1} dispersions in MeOH.

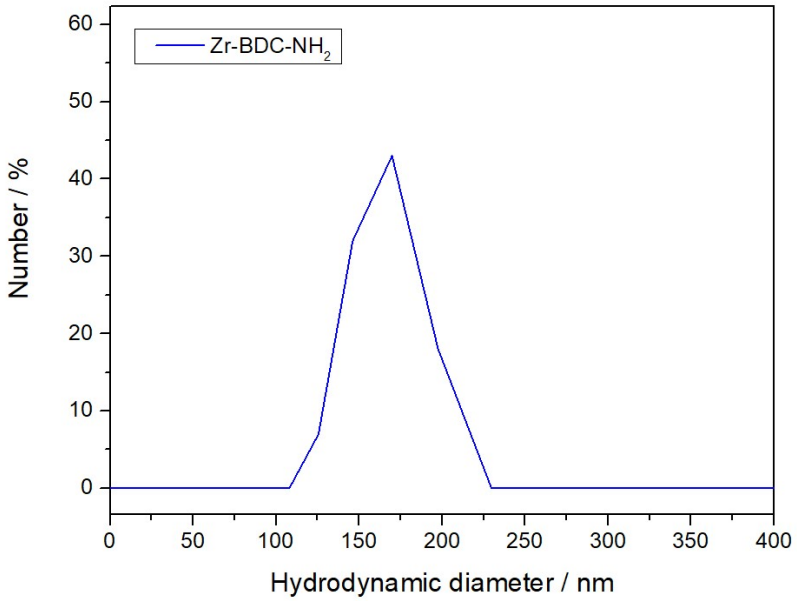

Figure S17: Hydrodynamic diameter of Zr-BDC-NH_2 determined by Dynamic Light Scattering measurements of *ca.* 0.1 mg mL^{-1} dispersions in MeOH.

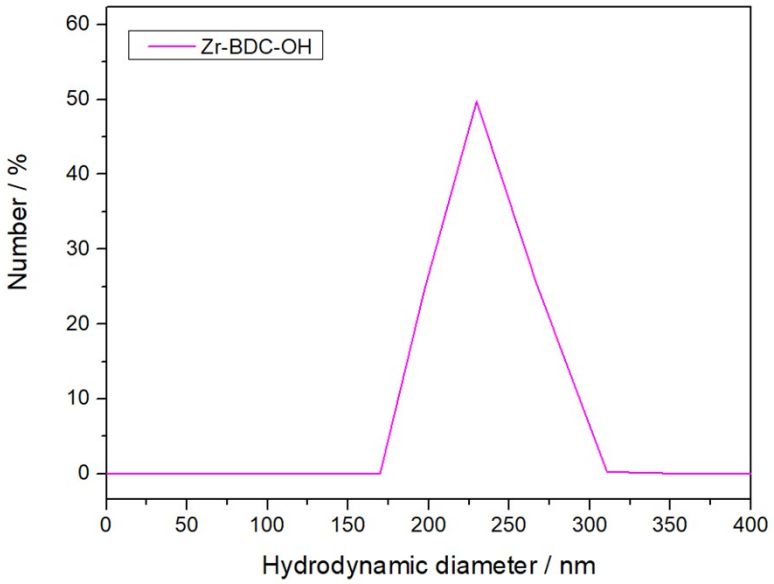

Figure S18: Hydrodynamic diameter of Zr-BDC-OH determined by Dynamic Light Scattering measurements of *ca.* 0.1 mg mL^{-1} dispersions in MeOH.

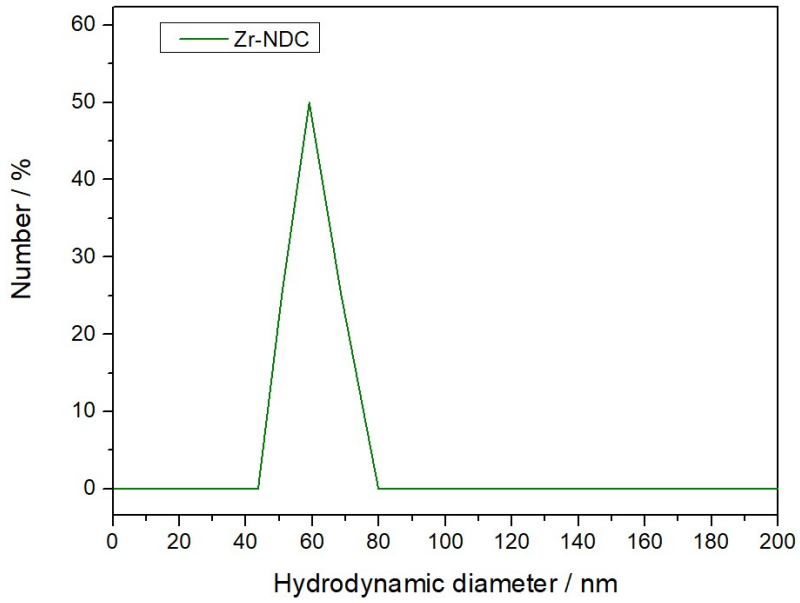

Figure S19: Hydrodynamic diameter of Zr-NDC determined by Dynamic Light Scattering measurements of *ca.* 0.1 mg mL^{-1} dispersions in MeOH.

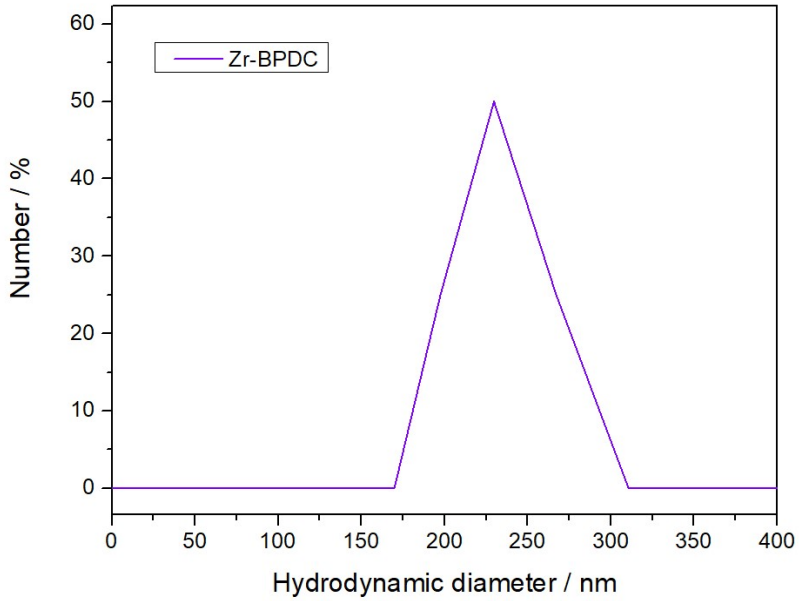

Figure S20: Hydrodynamic diameter of Zr-BPDC determined by Dynamic Light Scattering measurements of *ca.* 0.1 mg mL^{-1} dispersions in MeOH.

S.3.4. N_2 adsorption and desorption isotherms

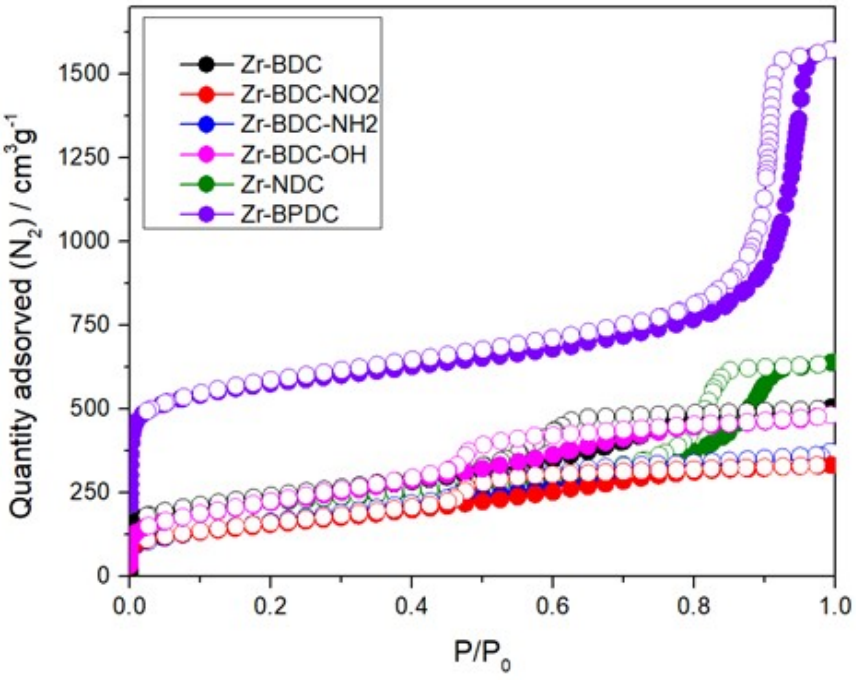

Figure S21: N_2 adsorption and desorption isotherms of ultra-small Zr-MOFs

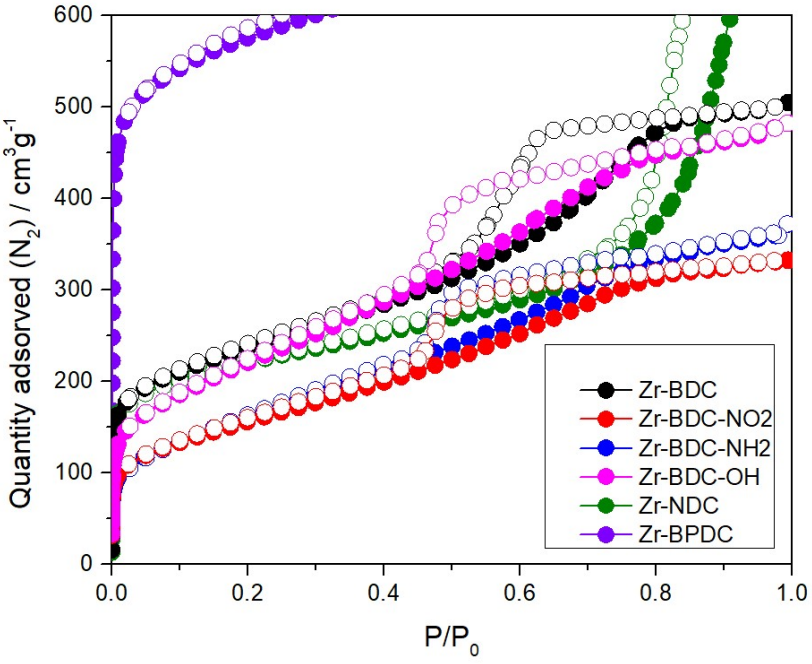

Figure S22: Amplification of N_2 adsorption and desorption isotherms of ultra-small Zr-MOFs showing hysteresis loops characteristic of mesoporous materials.

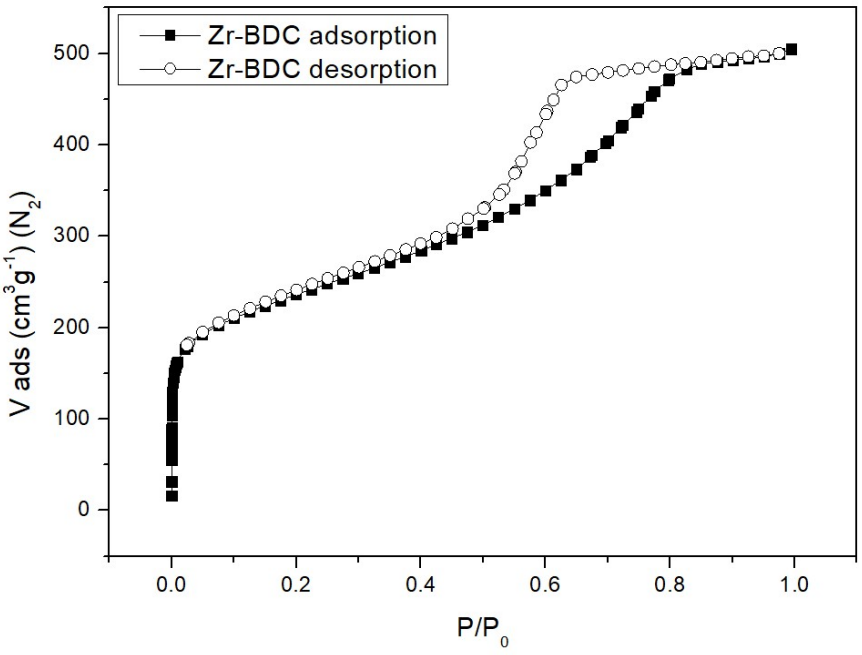

Figure S23: N_2 adsorption and desorption isotherm of ultra-small Zr-BDC showing hysteresis characteristic of mesoporous materials.

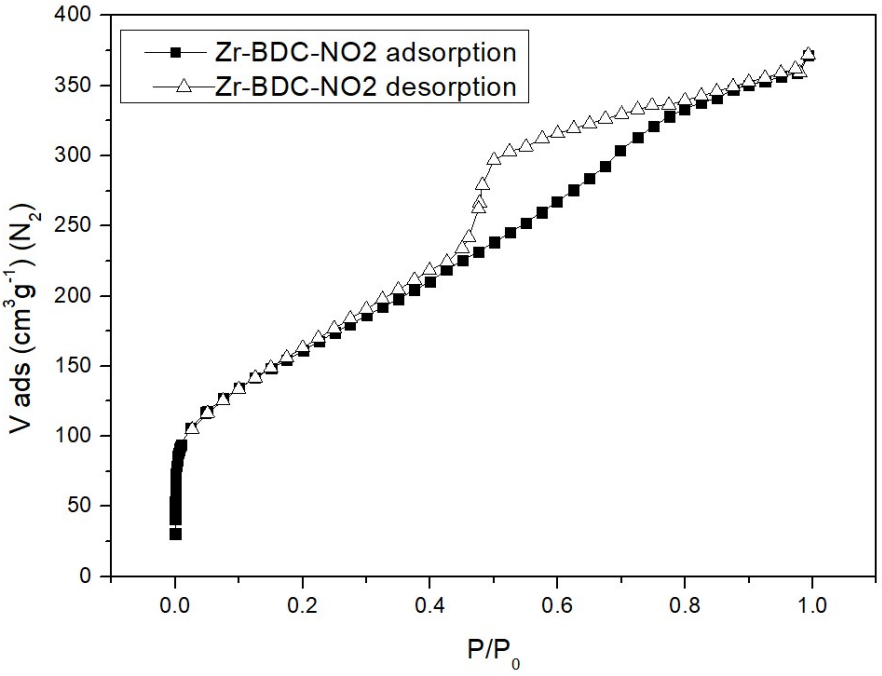

Figure S24: N_2 adsorption and desorption isotherm of ultra-small Zr-BDC-NO_2 showing hysteresis characteristic of mesoporous materials.

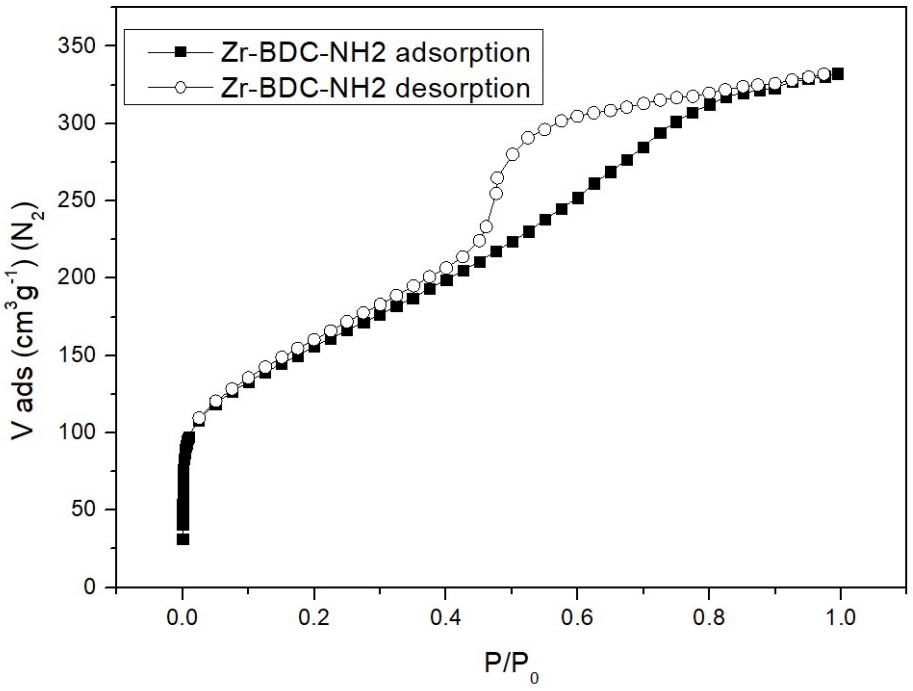

Figure S25: N_2 adsorption and desorption isotherm of ultra-small Zr-BDC-NH_2 showing hysteresis characteristic of mesoporous materials.

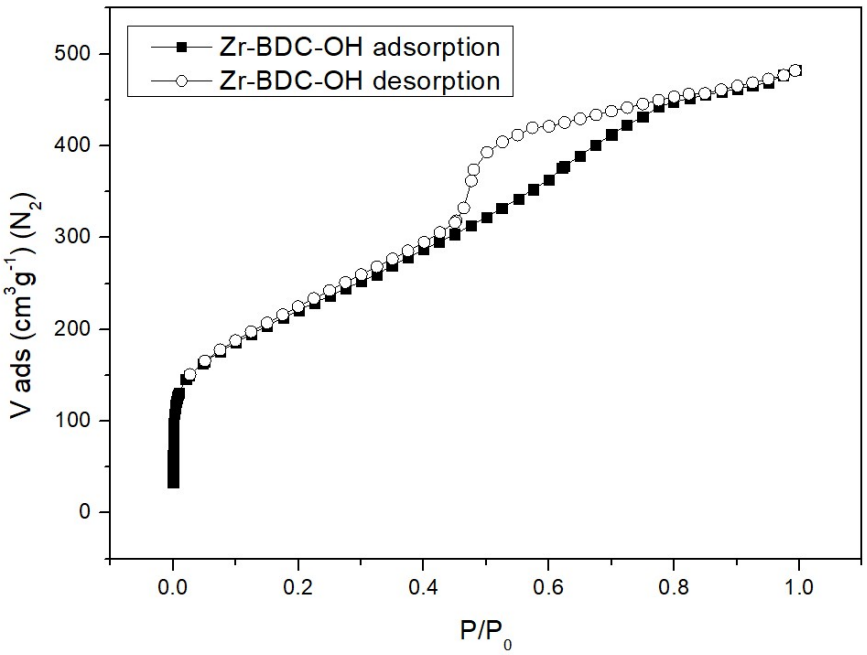

Figure S26: N_2 adsorption and desorption isotherm of ultra-small Zr-BDC-OH showing hysteresis characteristic of mesoporous materials.

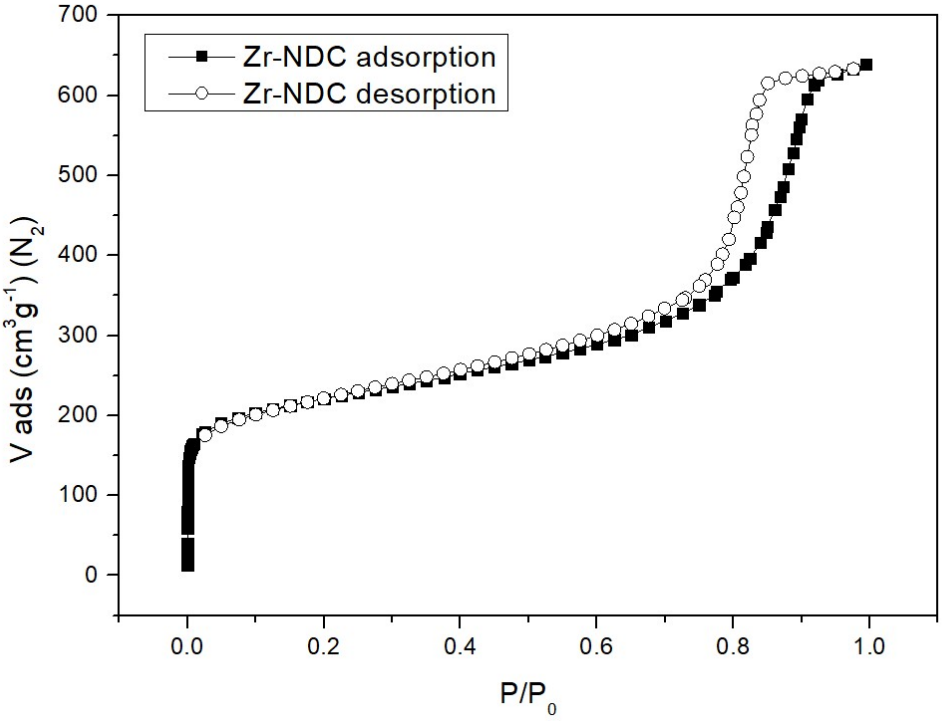

Figure S27: N_2 adsorption and desorption isotherm of ultra-small Zr-NDC showing hysteresis characteristic of mesoporous materials.

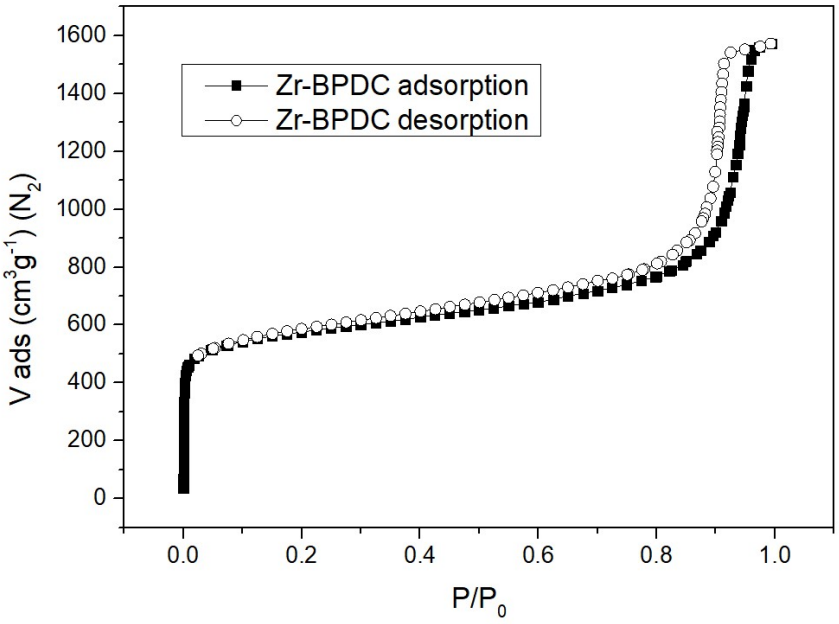

Figure S28: N_2 adsorption and desorption isotherm of ultra-small Zr-BPDC showing hysteresis characteristic of mesoporous materials.

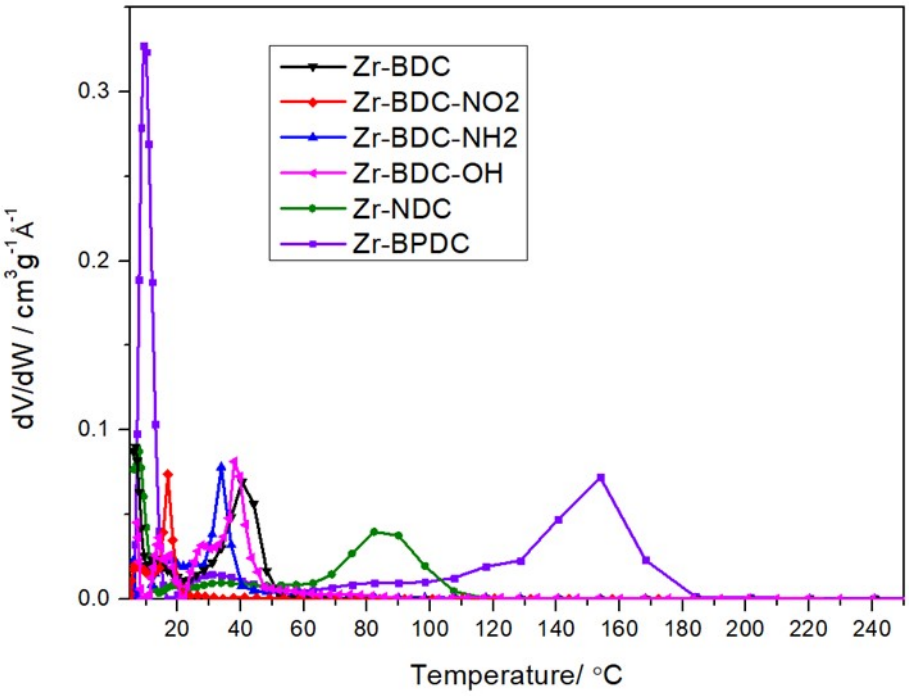

Figure S29: Pore size distributions extracted from the N_2 adsorption and desorption isotherms of ultra-small Zr-MOFs. Pore size distributions calculated with DFT Cylindrical oxide surface pore model.

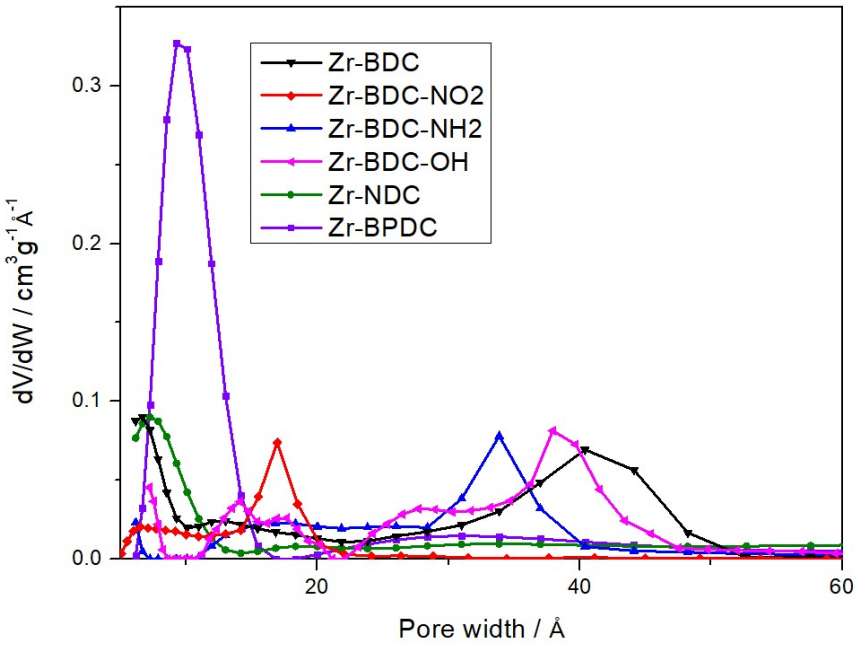

Figure S30: Pore size distributions extracted from the N_2 adsorption and desorption isotherms of ultra-small Zr-MOFs. Pore size distributions calculated with DFT Cylindrical oxide surface pore model.

Table S2: Tabulated data extracted from N_2 adsorption and desorption measurements of ultra-small Zr-MOFs.

Sample	BET Surface area	Total Pore volume	Micropore volume	mesopore volume	%mesopore volume
	m^2g^{-1}	cm^3g^{-1}	cm^3g^{-1}	cm^3g^{-1}	%
Zr-BDC	894	0.74	0.25	0.48	65.9
Zr-BDC-OH	452	0.49	0.45	0.04	7.9
Zr-BDC-NO_2	484	0.53	0.15	0.38	71.5
Zr-BDC-NH_2	593	0.69	0.17	0.52	75.5
Zr-NDC	769	0.94	0.24	0.71	75.0
Zr-BPDC	2006	2.33	0.74	1.59	68.3

S.3.5. FT-IR

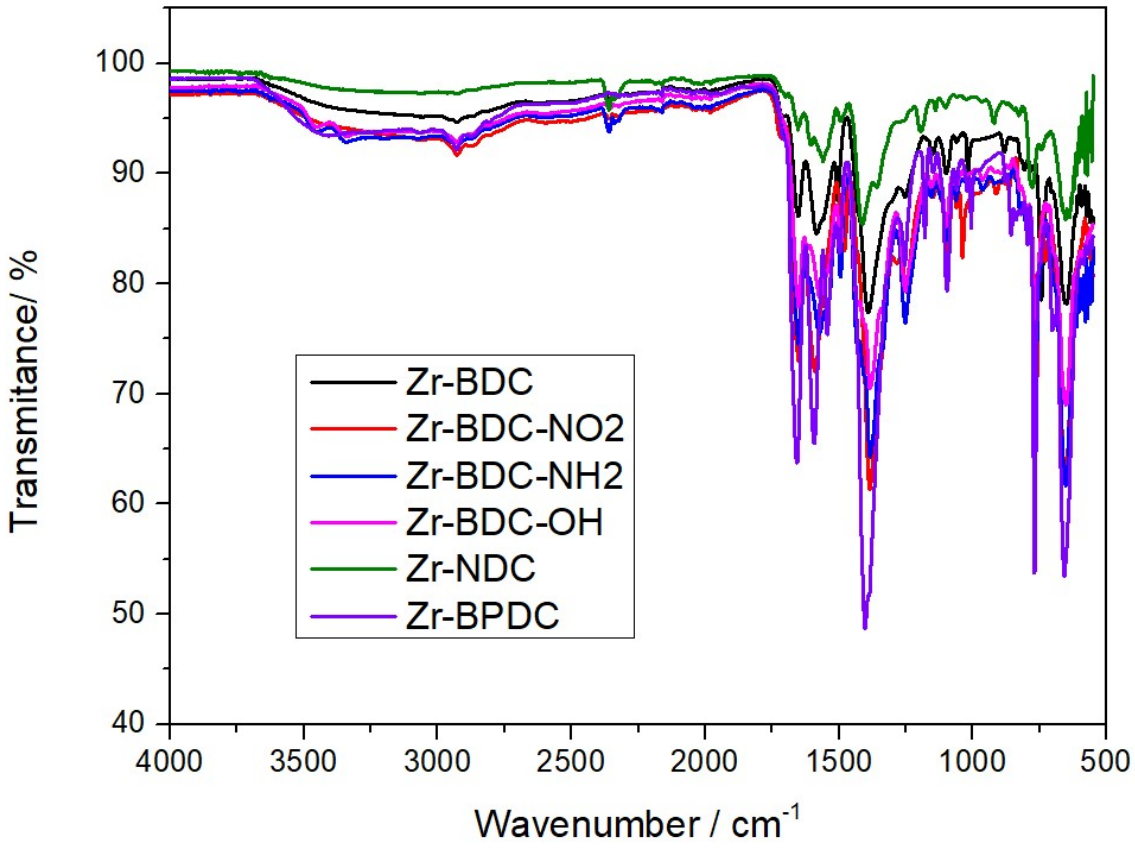

Figure S31: Raw FT-IR profiles of ultra-small Zr-MOF.

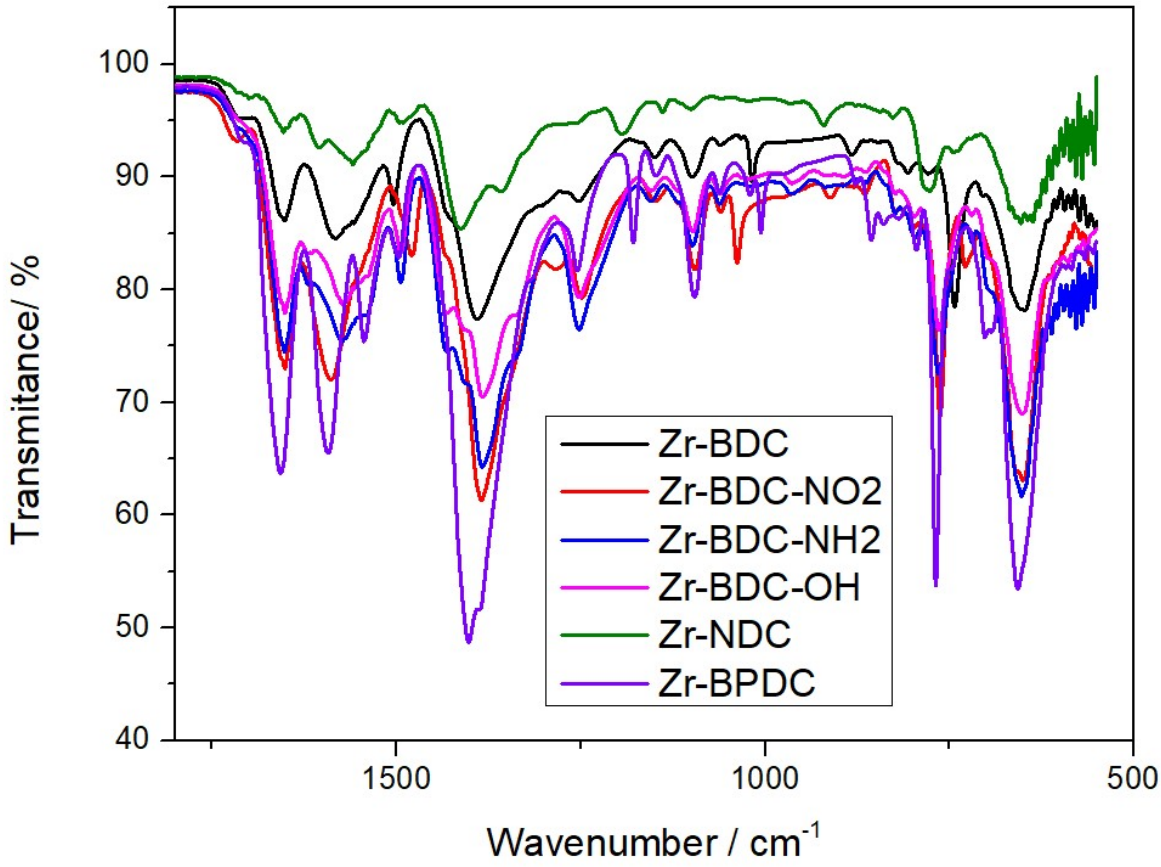

Figure S32: Amplification of raw FT-IR profiles of ultra-small Zr-MOF.

S.3.6. ^{1}H-NMR Spectroscopic data

Formic acid coming from the decomposition of DMF during synthesis was present in the ^{1}H NMR spectra alongside with the modulator AcOH and DMF, possibly bonded to metals in the structure as defect-compensating ligand. Incorporation of modulator and formic acid is expressed as the **molar ratio** ($R_{mod,}$) between modulator and bdc (Equation 1) and as the **molar percent** of modulator (mol%) compared to bdc (Equation 2), while the **total modulator percent** (total mod%) is calculated taking into account modulator, formic acid and bdc (Equation 3).

Equation 1: molar ratio ($R_{mod,}$) between modulator and bdc.

$$Rmod = \frac{Mod}{bdc}$$

Equation 2: molar percent of modulator (mol%) compared to bdc.

$$mol\% = \frac{Mod}{Mod + bdc} * 100$$

Equation 3: total modulator percent (total mod%).

$$total\ mod\% = \frac{Mod + FA}{Mod + FA + bdc} * 100$$

Table S3: Tabulated data extracted from ^{1}H NMR spectra of acid digested ultra-small Zr-MOFs as molar ratio (r mod) and molar percent (% mod)

	r acoh	rfa	rdmf	%acoh	%fa	%dmf
Zr-BDC	0.179	0.081	0.436	15.2	7.5	30.4
Zr-BDC-OH	0.404	0.755	0.091	28.8	43.0	8.3
Zr-BDC-NO_2	1.058	0.294	0.143	51.4	22.7	12.5
Zr-BDC-NH_2	0.392	0.118	0.324	28.2	10.6	24.5
Zr-NDC	0.180	0.178	0.427	15.3	15.1	29.9
Zr-BPDC	0.147	0.674	1.463	12.8	40.3	59.4

Note that formic acid comes from the decomposition of DMF during synthesis. [1]

S.3.7. Thermogravimetric Analysis

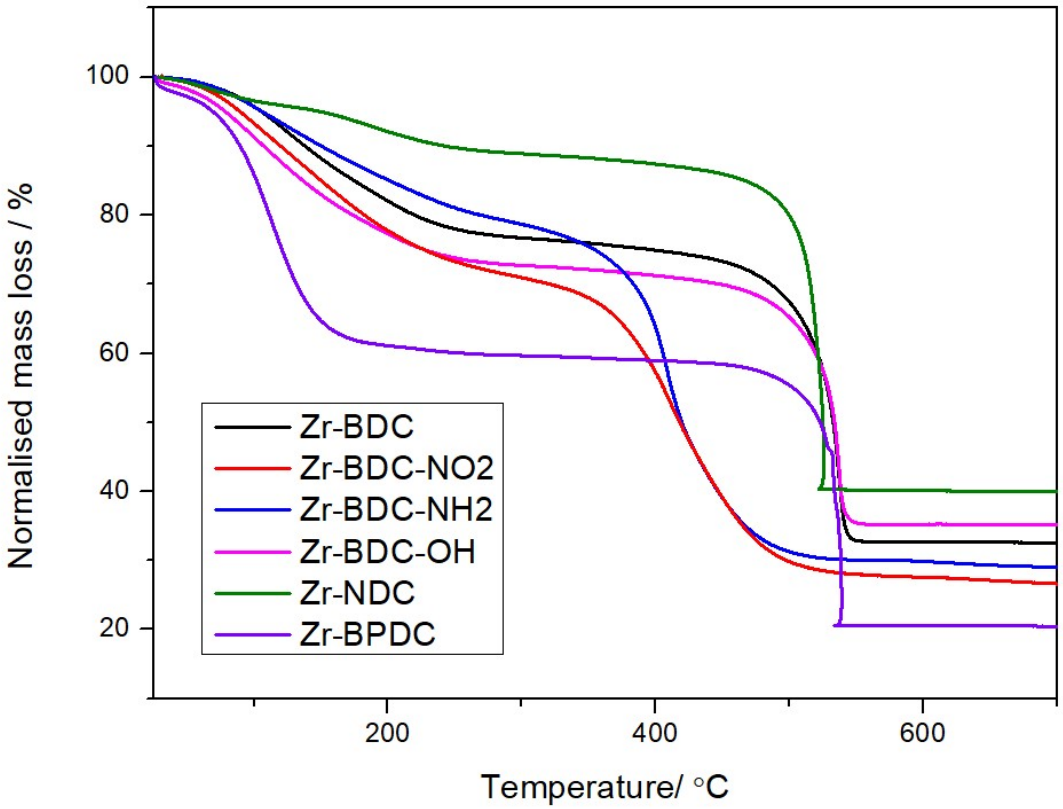

Figure S33: TGA profiles of ultra-small Zr-MOF, with the start of the decomposition profiles normalised to 100%.

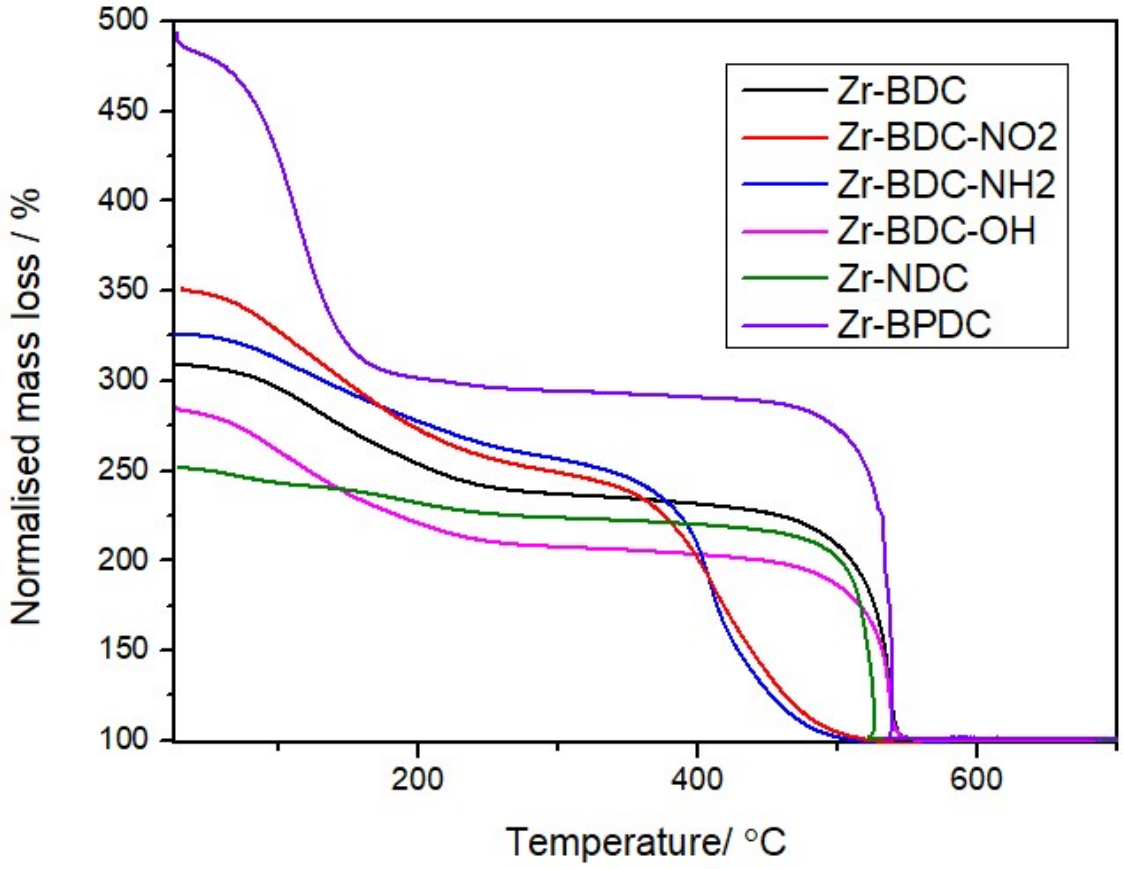

Figure S34: TGA profiles of ultra-small Zr-MOF, with the residues normalised to 100%.

Due to the clear start of the dehydrated MOF (DH MOF) decomposition profile (prior to the decomposition of linkers, at *ca.* 400°C) and to the presence of DMF molecules (characterized by ^{1}H NMR spectroscopy) that could be paired with defect-compensating OH^- molecules to balance the coordination number of the metals, we have analyzed the thermal decomposition profiles to obtain the number of linkers in the structures based on the mass ration between the DH MOF and the thermal residue (R_{expDH}). It is important to note that both FA, AcOH and DMF decompose before the DH MOF leading to the $ZrOL_xO_{1-x}$ structure. Hence, the formula will be: [2]

$$R_{expDH} = \frac{M_w\,[DH\ MOF]}{M_w\ [Residue]} = \frac{M_w\ [ZrO(L)_xO_{1-x}]}{M_w\ [ZrO_2]}$$

Then,

$$X\ Ligands = \frac{\left(R_{expDH} * M_w\left[\,ZrO_2\right]\right) - M_w\ [ZrO] - M_w\,[O]}{M_w\,[L] - M_w\,[O]}$$

Once the number of linkers in the structure has been calculated, the number of modulators (FA and ACOH) are obtained by multiplying the number of linker by the mod/L molar ratio determined by ^{1}H NMR spectroscopy (Table S3).

Then, the number of OH- molecules compensating for the charge arising from the missing linkers is calculated using the charge balance equation.

$$4\ (Charge\ Zr) = \frac{4}{6} * 2\ O + \frac{4}{6} * OH + 2 * X\ Ligand + Y\ Mod1 + Z\ Mod2 + D\ OH\ ;$$

$$D\ OH = 2 - 2 * X\ Ligand - y\ Mod1 - z\ Mod\ 2$$

The values of R_{exp} and R_{expDH} are given in **Table S4**, and the composition values obtained by this method in **Tables S4** and **S5**.

Table S4: Rexp and RexpDH values extracted from TGA analysis.

SAMPLE	R_{EXP}	R_{EXPDH}	L/Zr
Zr-BDC	3.0248	2.1700	0.973
Zr-BDC-OH	3.46	2.27	0.810
Zr-BDC-NO_2	3.88	2.31	0.989
Zr-BDC-NH_2	2.84	2.04	0.781
Zr-NDC	2.52	2.24	0.771
Zr-BPDC	4.8	2.79	0.984

Table S5: Data extracted from TGA analysis for the model framework $(Zr_6O_6(OH)_6(L)_X(AcOH)y(FA)z$

SAMPLE	PKA_1	6nL	6n FA	6nAcOH	%ML	OH / H_2O
Zr-BDC	3.51	5.839	0.472	1.048	2.681	-1.198
Zr-BDC-OH	1.73	4.861	3.668	1.964	18.976	-3.355
Zr-BDC-NO_2	3.95	5.936	1.743	6.282	1.066	-7.897
Zr-BDC-NH_2	2.56	4.684	0.551	1.837	21.927	0.243
Zr-NDC	3.69	4.625	0.825	0.833	22.910	1.091
Zr-BPDC	3.77	5.902	3.978	0.867	1.639	-4.648

It is important to take into account that since the particle size is very small, linker and/or modulators could be terminating the surfaces, which in this case are a highly relevant percent in the material, thus hindering the accurate compositional results. The values obtained for linker composition are more accurate as those are based in the R_{expDH} step of the thermal decomposition profile. Multiplying these values by the ^1H NMR spectroscopic ratios obtained for FA and OH modulators show that either FA, AcOH and/or the linkers are terminating the ultra-small nanoparticles surface, those giving higher coordination numbers than expected and resultant OH^-/H_2O negative values.

S.4. Catalytic activity

Kinetic study of the formylation of aniline

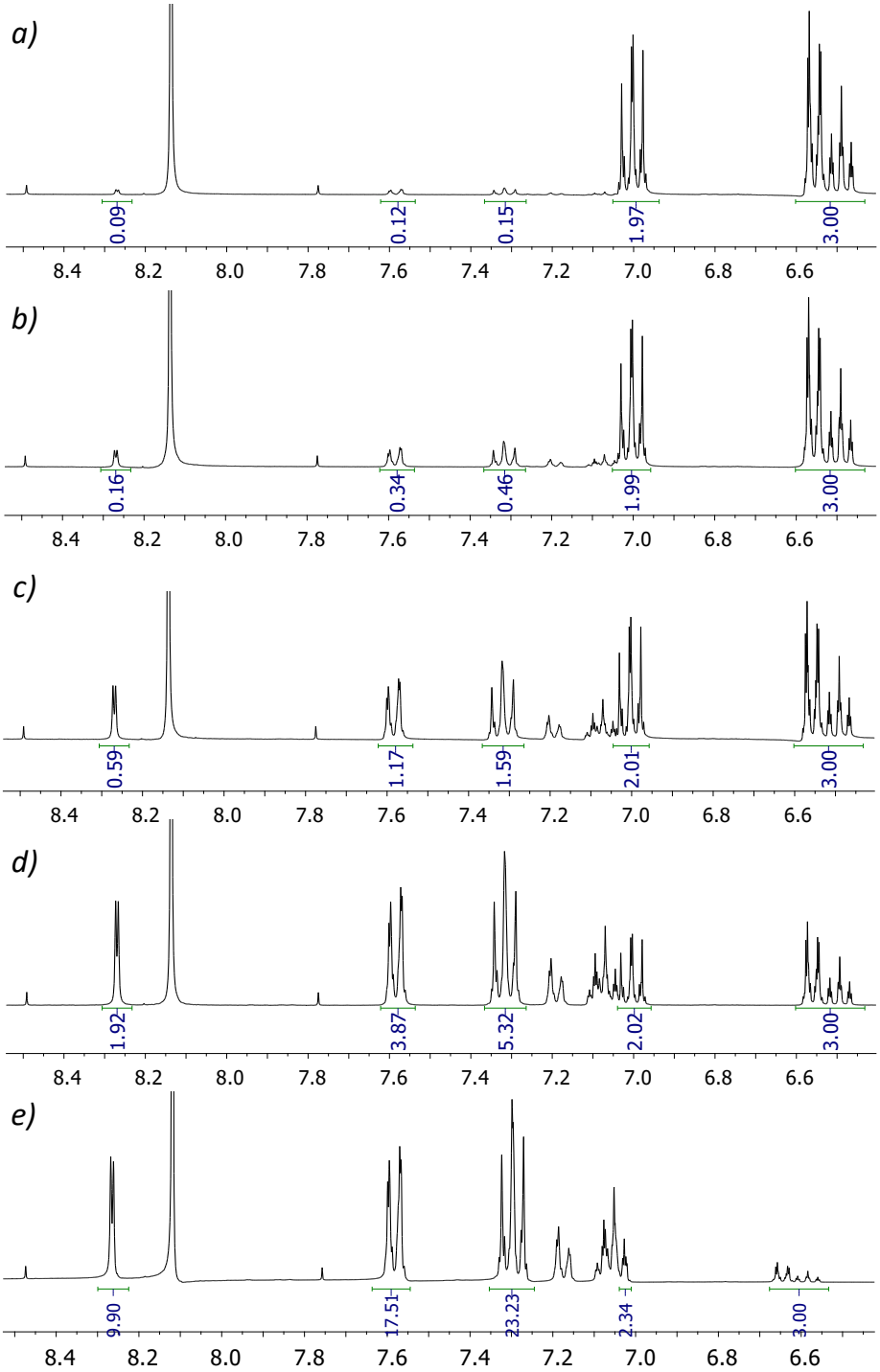

Figure S35. ^{1}H-NMR spectra (aromatic region) after 1 min (a), 8 min (b), 1h (c), 4h (d) and 1 day (e) of reaction between aniline (100 µL) and formic acid (200 µL) under solvent-free conditions at 35 ºC in presence of MOF Zr-BDC-NH_2 (10 mg).

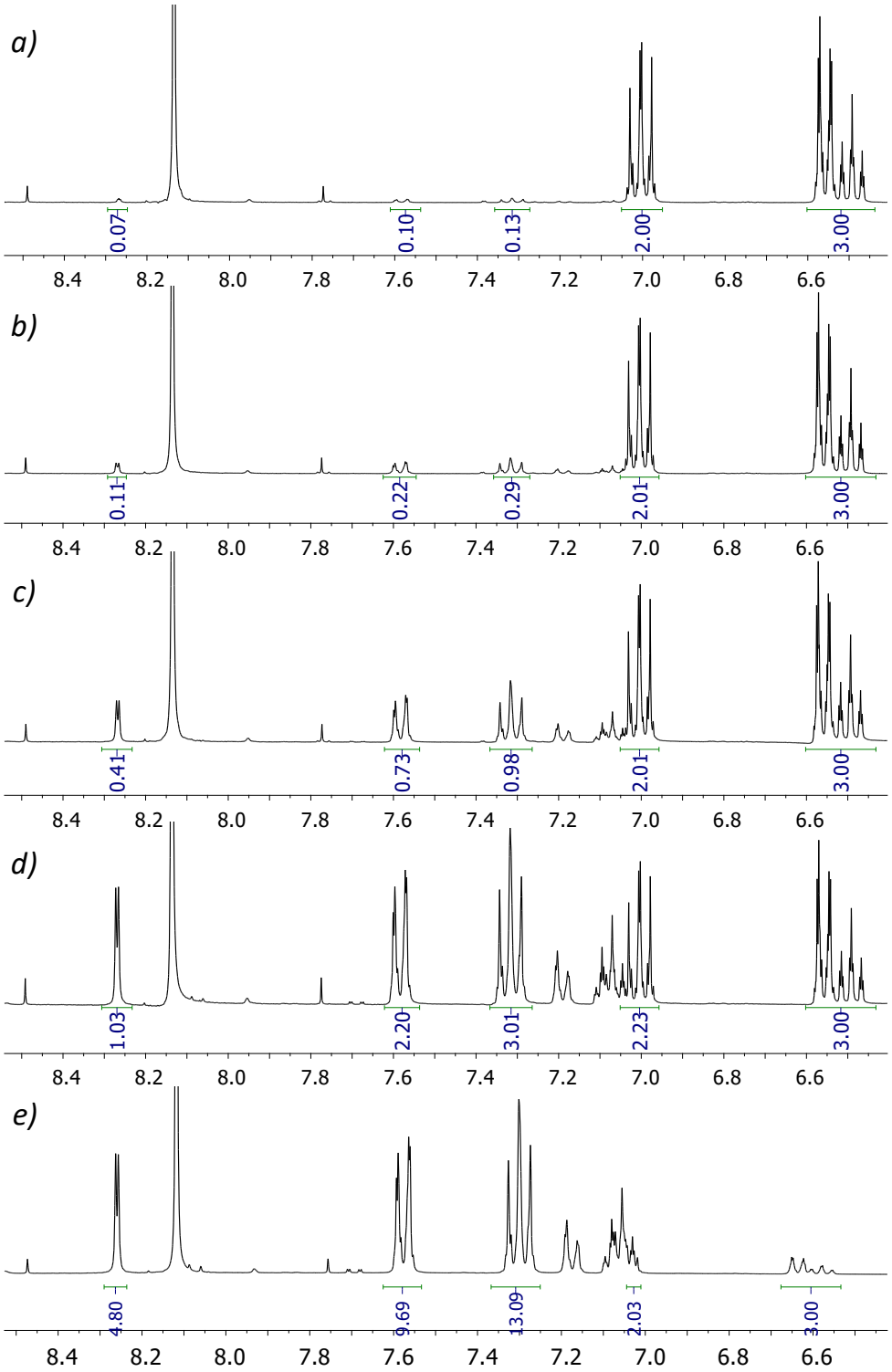

Figure S36. ^{1}H-NMR spectra (aromatic region) after 1 min (a), 8 min (b), 1h (c), 4h (d) and 1 day (e) of reaction between aniline (100 µL) and formic acid (200 µL) under solvent-free conditions at 35 ºC in absence of MOF.

Table S6. Kinetic study of the solvent-free formylation of aniline (100 µL) with formic acid (200 µL) at 35ºC in the presence or absence (blank) of Zr-BDC-NH_2 (10 mg).

Time/h	Yield/%	
	Zr-BDC-NH_2	Blank
0.02	5	4
0.13	13	9
1	34	25
4	64	50
24	89	81

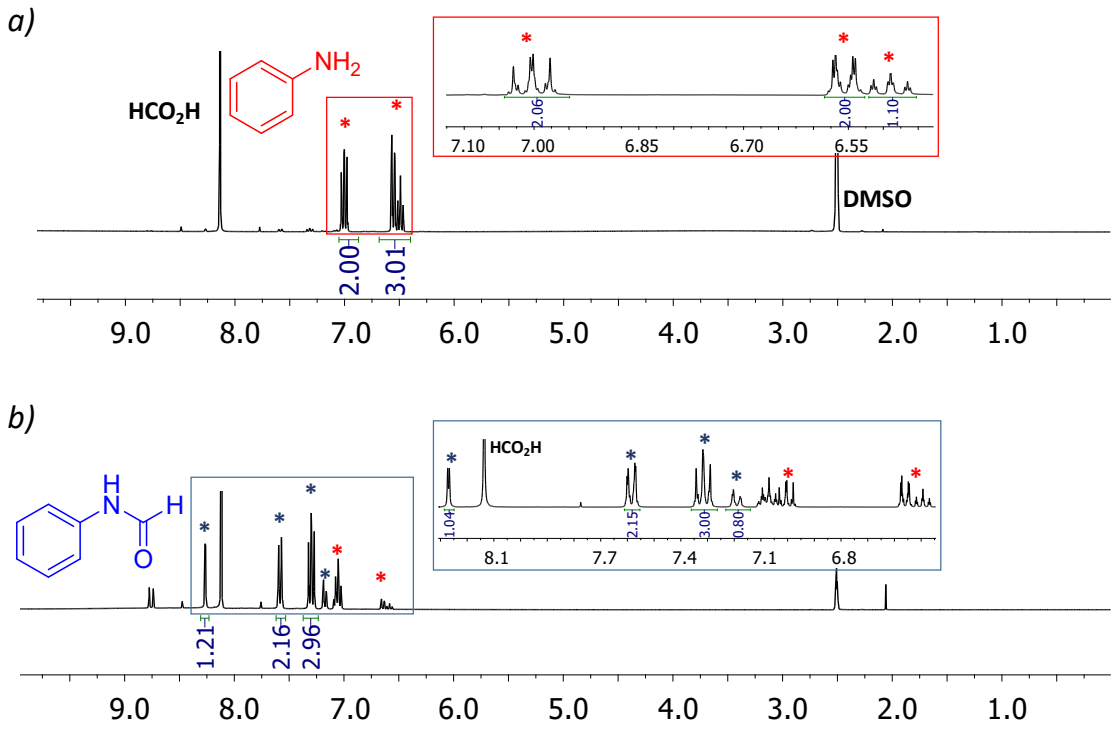

Figure S37. ^{1}H-NMR (300 MHz, DMSO) spectra of the (a) starting aniline (*) and formic acid (in a 1:2 volume or 5 eq. excess) after 1 min of reaction (see zoom of the aromatic region at the right part) and (b) 89% yield *N*-Phenyl formamide product (*) after 24 h of reaction (see zoom of the aromatic region at the right part). (a) δ 7.08-6.93 (m, 2H, Ar_{orto}-H), 6.61-6.45 (m, 3H, $Ar_{meta,para}$-H). (b) δ 8.33-8.22 (brs, 1H, OC-H), 7.58 (m, 2H, Ar_{orto}-H), 7.39-7.25 (m, 3H, $Ar_{meta,para}$-H), 7.19 (brs, 1H, N-H).

Initial reaction rates

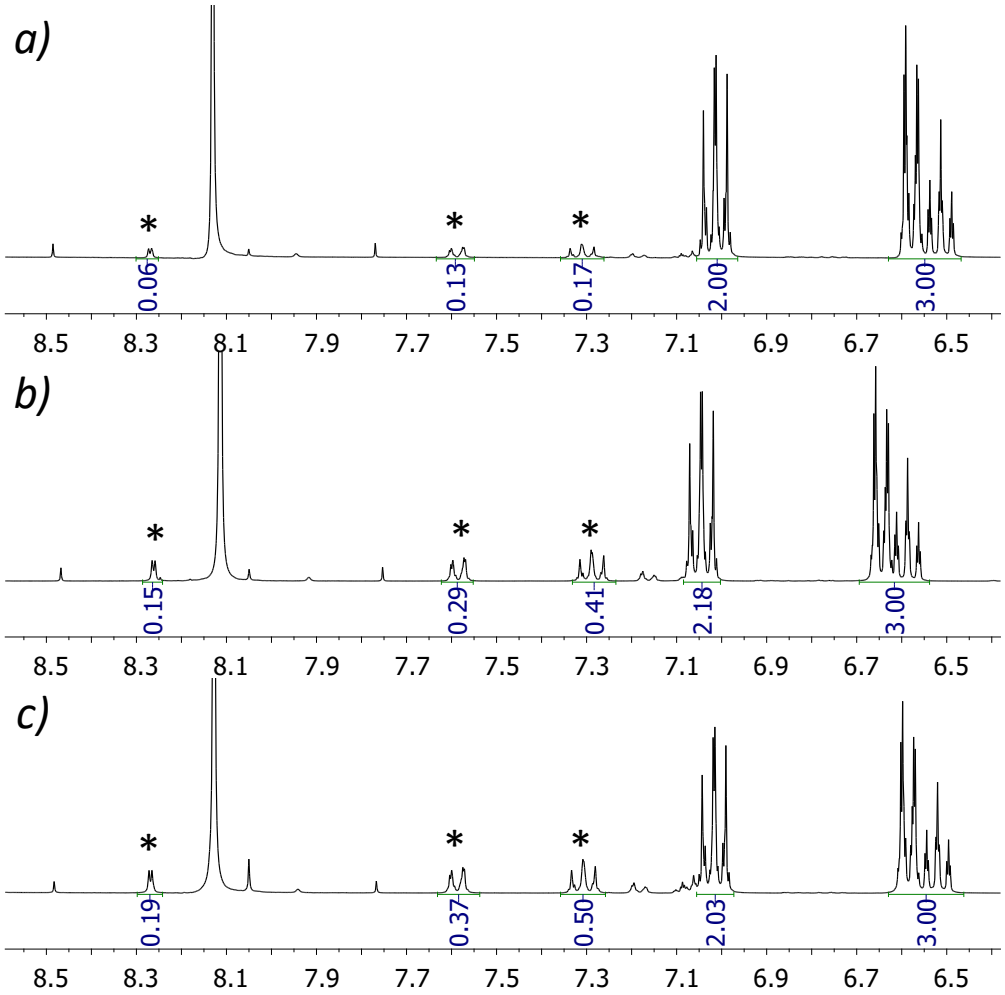

Figure S38. ^{1}H-NMR spectra (aromatic region) after 2 min (a), 5 min (b) and 10 min (c) of reaction between aniline and formic acid under solvent-free conditions in the presence of Zr-BDC. Reaction conditions: 5 eq. of acid, 10%wt. MOF, 35 ºC.

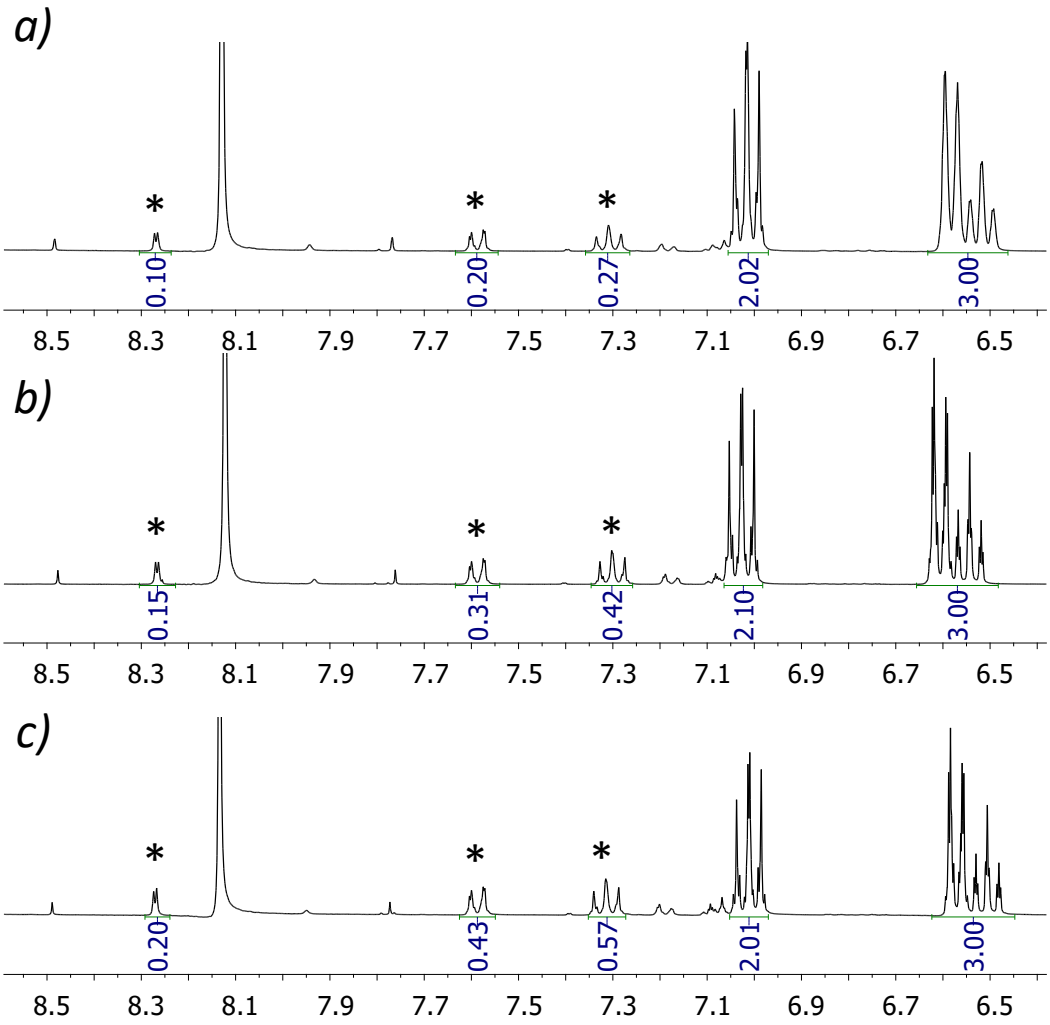

Figure S39. ^{1}H-NMR spectra (aromatic region) after 2 min (a), 5 min (b) and 10 min (c) of reaction between aniline and formic acid under solvent-free conditions in the presence of Zr-BDC-NH_2. Reaction conditions: 5 eq. of acid, 10%wt. MOF, 35 ºC.

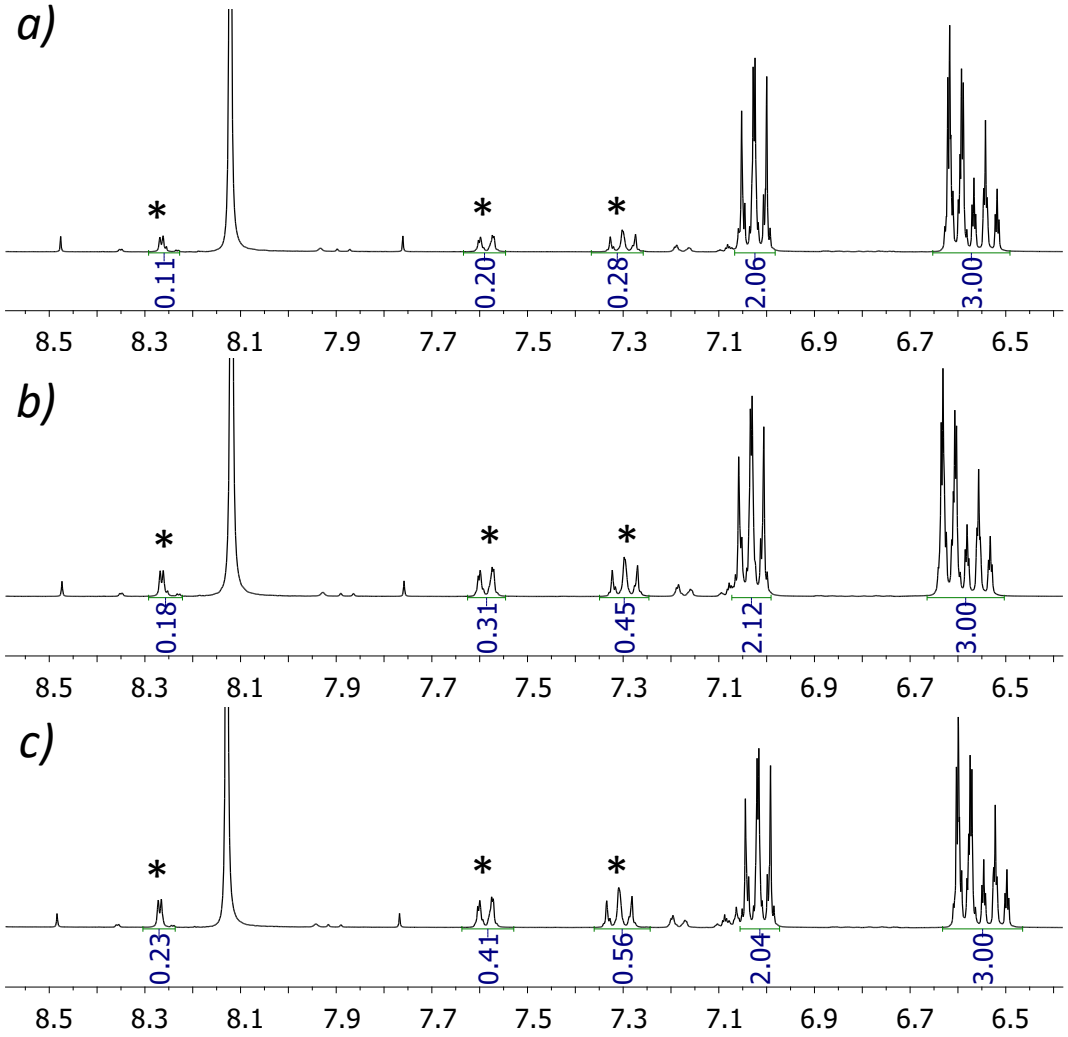

Figure S40. ^{1}H-NMR spectra (aromatic region) after 2 min (a), 5 min (b) and 10 min (c) of reaction between aniline and formic acid under solvent-free conditions in the presence of Zr-BDC-NO_2. Reaction conditions: 5 eq. of acid, 10%wt. MOF, 35 ºC.

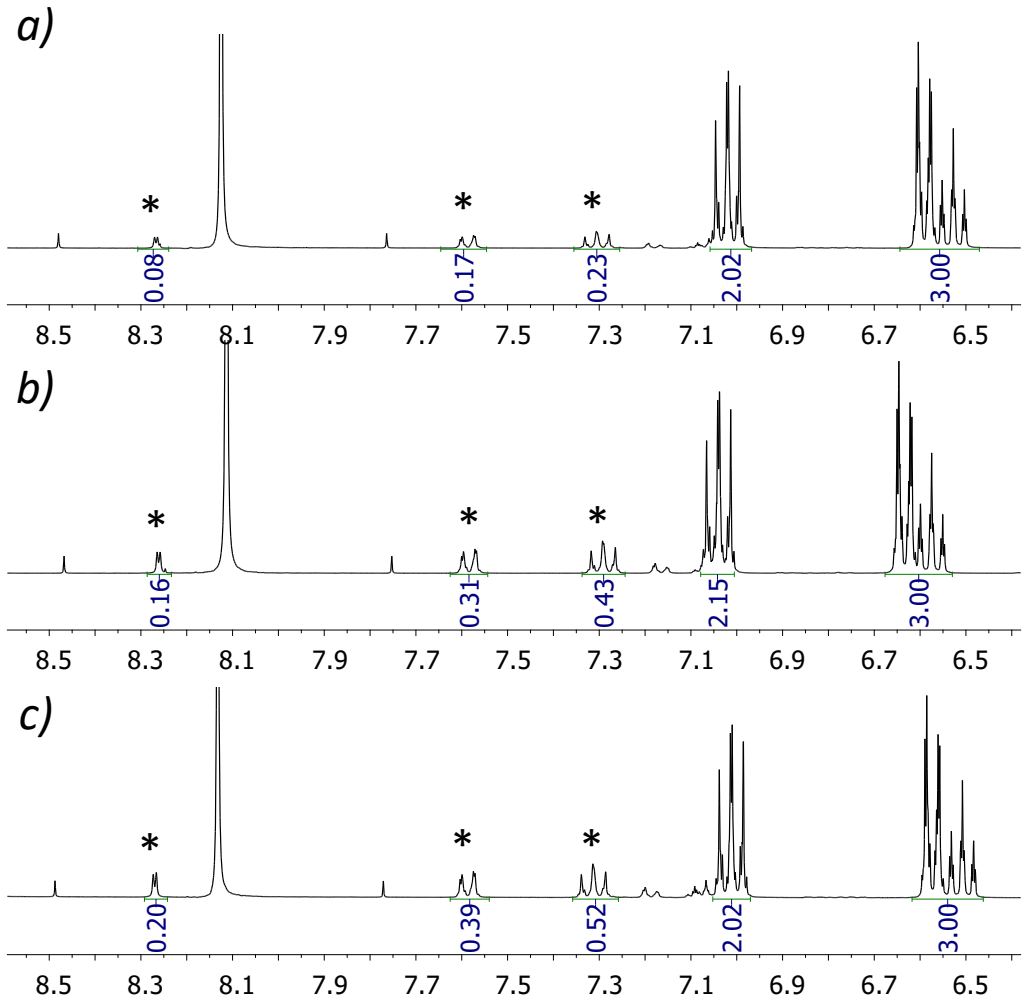

Figure S41. ^{1}H-NMR spectra (aromatic region) after 2 min (a), 5 min (b) and 10 min (c) of reaction between aniline and formic acid under solvent-free conditions in absence of MOF. Reaction conditions: 5 eq. of acid, 35 ºC.

Table S7. Beginning of the solvent-free formylation of aniline (see Figs. S38-41) at 35ºC under similar conditions to those of Table S6 for the calculation of initial reaction rates (r_0).

Sample	Yield/ % (time/ min)	r_0/ mmol·h^{-1}
Zr-BDC	5% (2 min), 12% (5 min), 14% (10 min)	1.7
Zr-BDC-NO_2	9% (2 min), 13% (5 min), 16% (10 min)	3.0
Zr-BDC-NH_2	9% (2 min), 13% (5 min), 16% (10 min)	3.0
Zr-BDC-OH	<7% (2 min)	<2.3
Zr-NDC	<7% (2 min)	<2.3
Zr-BPDC	<7% (2 min)	<2.3
blank	7% (2 min), 13% (5 min), 14% (10 min)	2.3

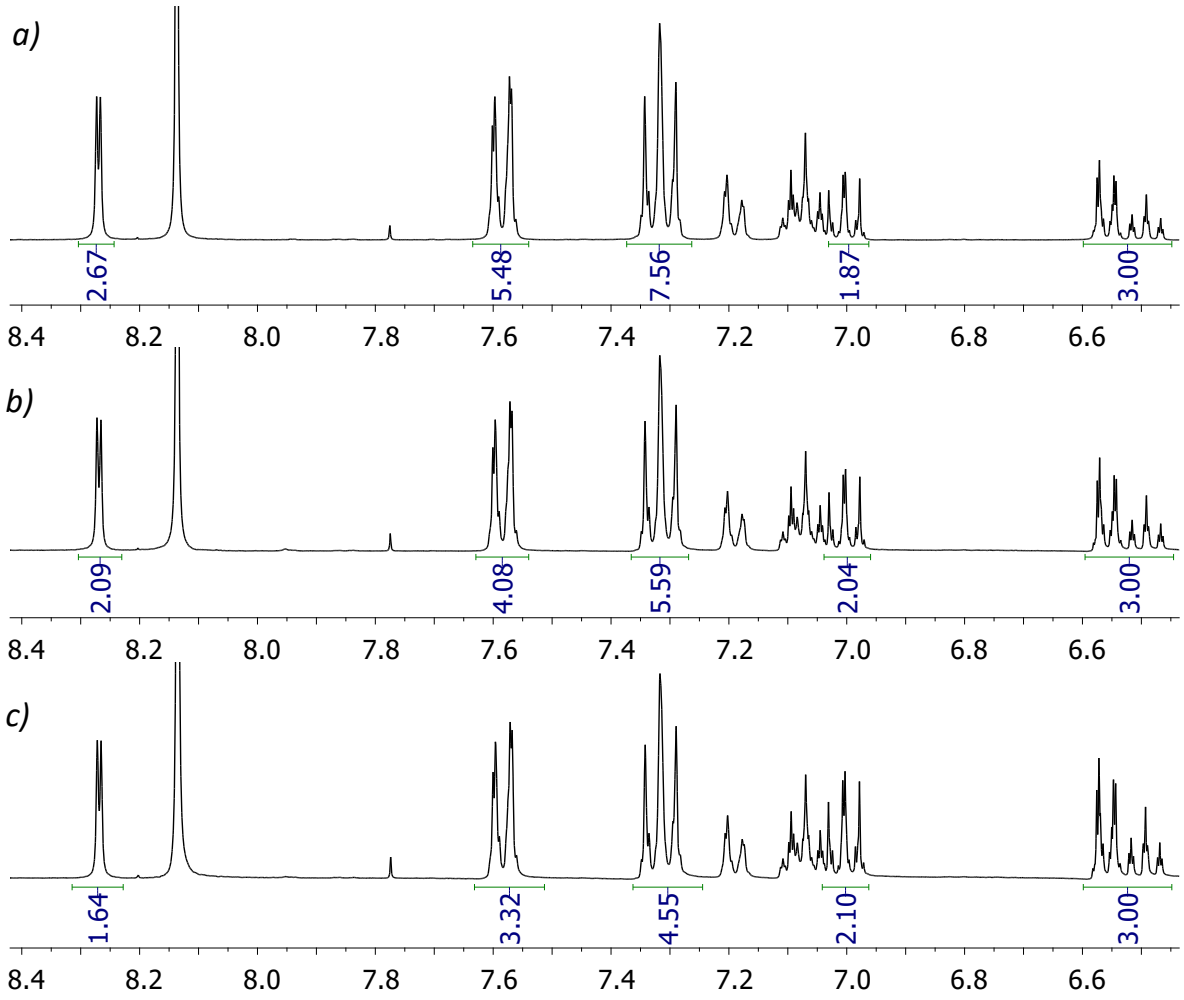

Figure S42. ^{1}H-NMR spectra (aromatic region) after 1st (a), 2nd (b) and 3rd (c) reaction cycles between aniline and formic acid under solvent-free conditions in presence of Zr-BDC-NH_2.

Table S8. Recyclability and leaching of Zr-BDC-NH_2 in the solvent-free formylation of aniline at 35ºC.[a]

Run	Yield/%	Zr/ wt% total Zr[b]	Zr/ wt % sample[c]
1	72	1.57	0.41
2	65	1.14	0.30
3	52	1.93	0.50

[a] 30 mg MOF Zr-BDC-NH_2, 200 µL aniline and 400 µL formic, 35 ºC. Reaction time: 30 min. [b] considering only the Zr amount of the fresh MOF. [c] Considering the total mass of the MOF sample.

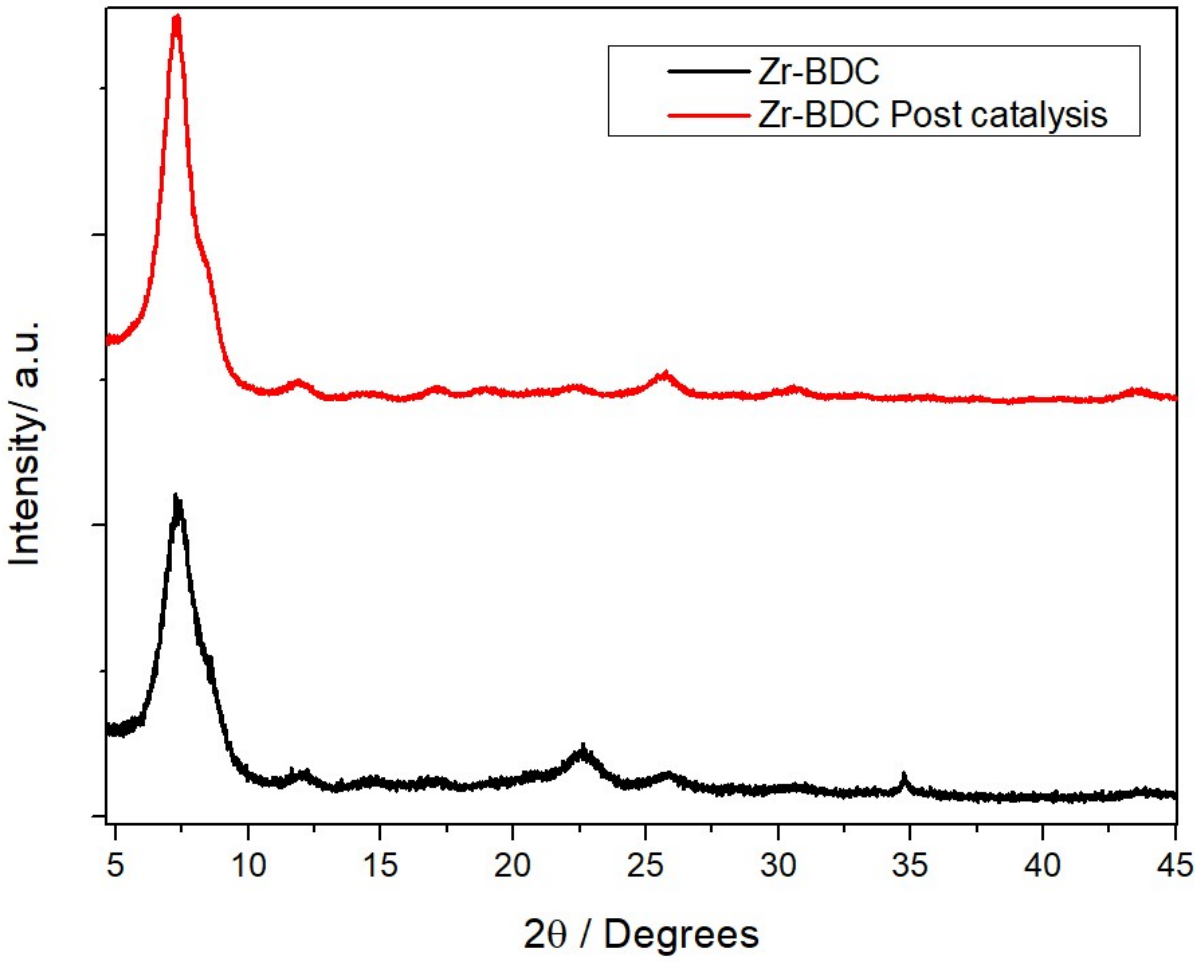

Figure S43: PXRD patterns of the ultra-small Zr-BDC MOF before and after 10 minutes of catalytic reaction with formic acid.

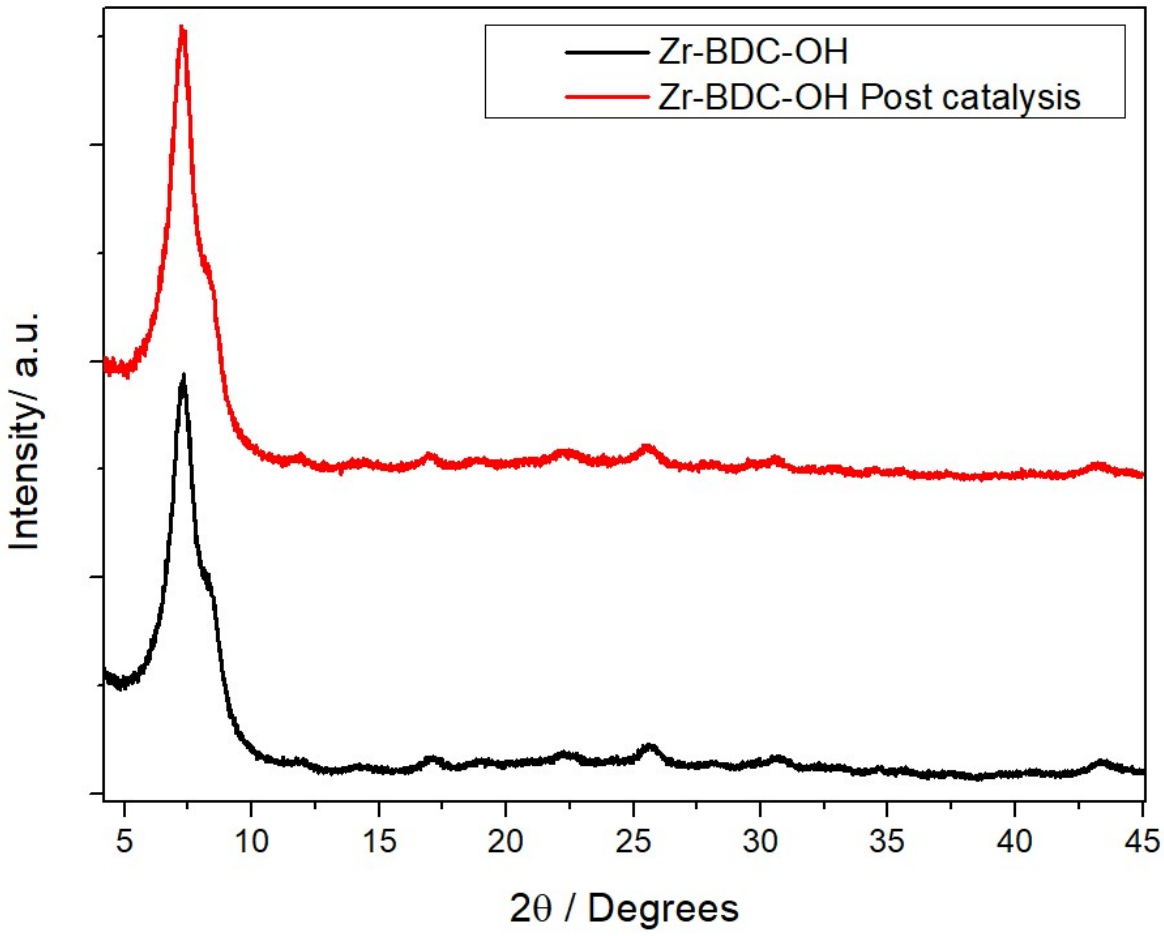

Figure S44: PXRD patterns of the ultra-small Zr-BDC-OH MOF before and after 10 minutes of catalytic reaction with formic acid.

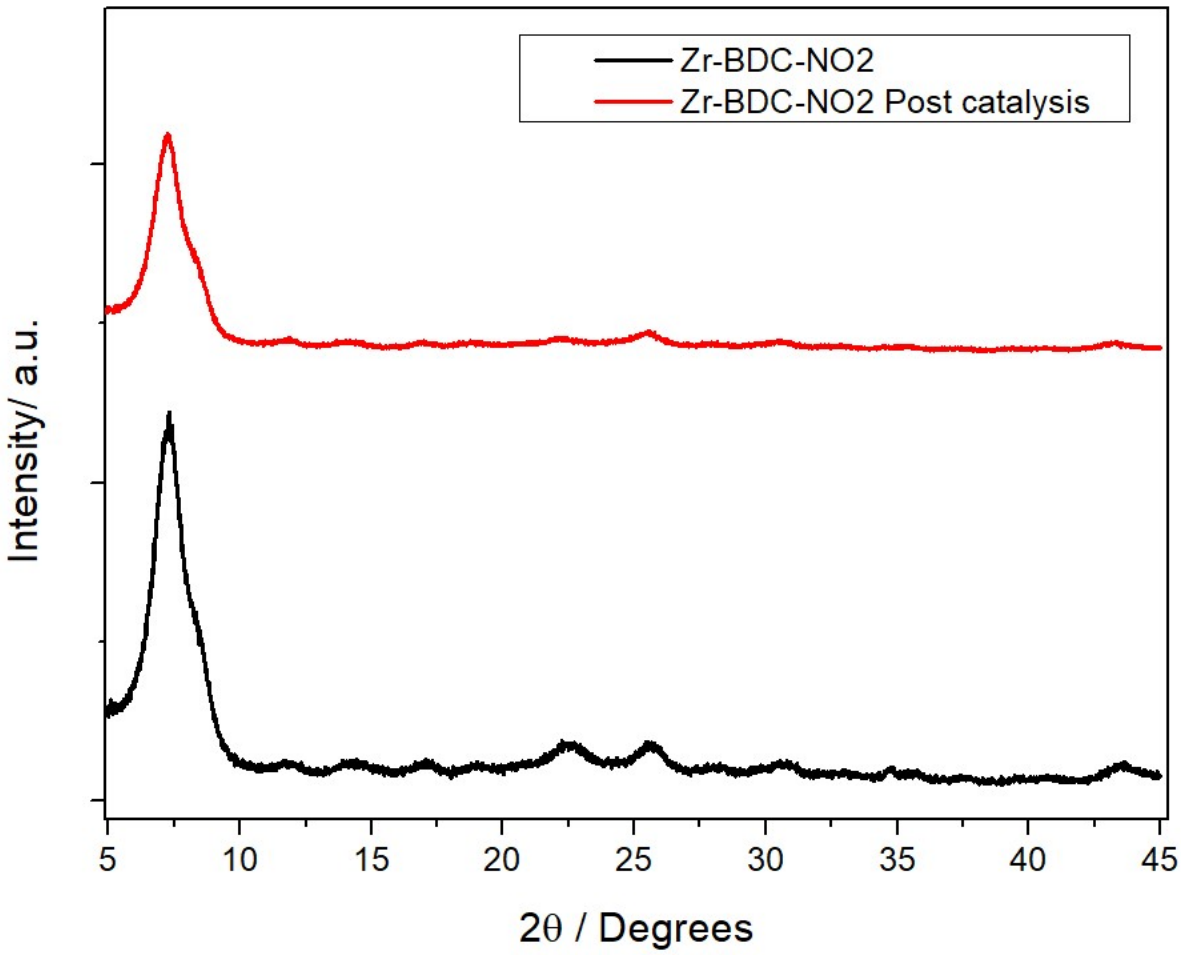

Figure S45: PXRD patterns of the ultra-small Zr-BDC-NO_2 MOF before and after the catalytic reaction.

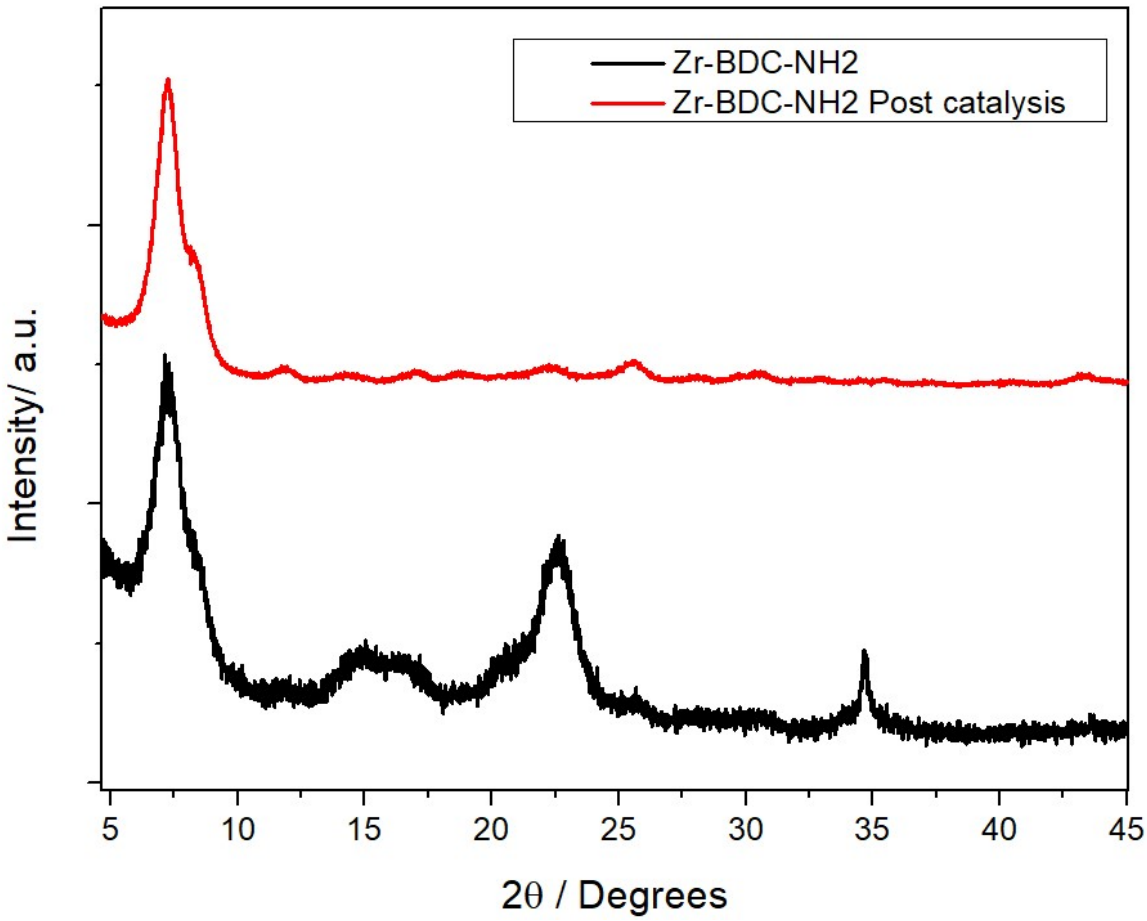

Figure S46: PXRD patterns of the ultra-small Zr-BDC-NH_2 MOF before and after the catalytic reaction.

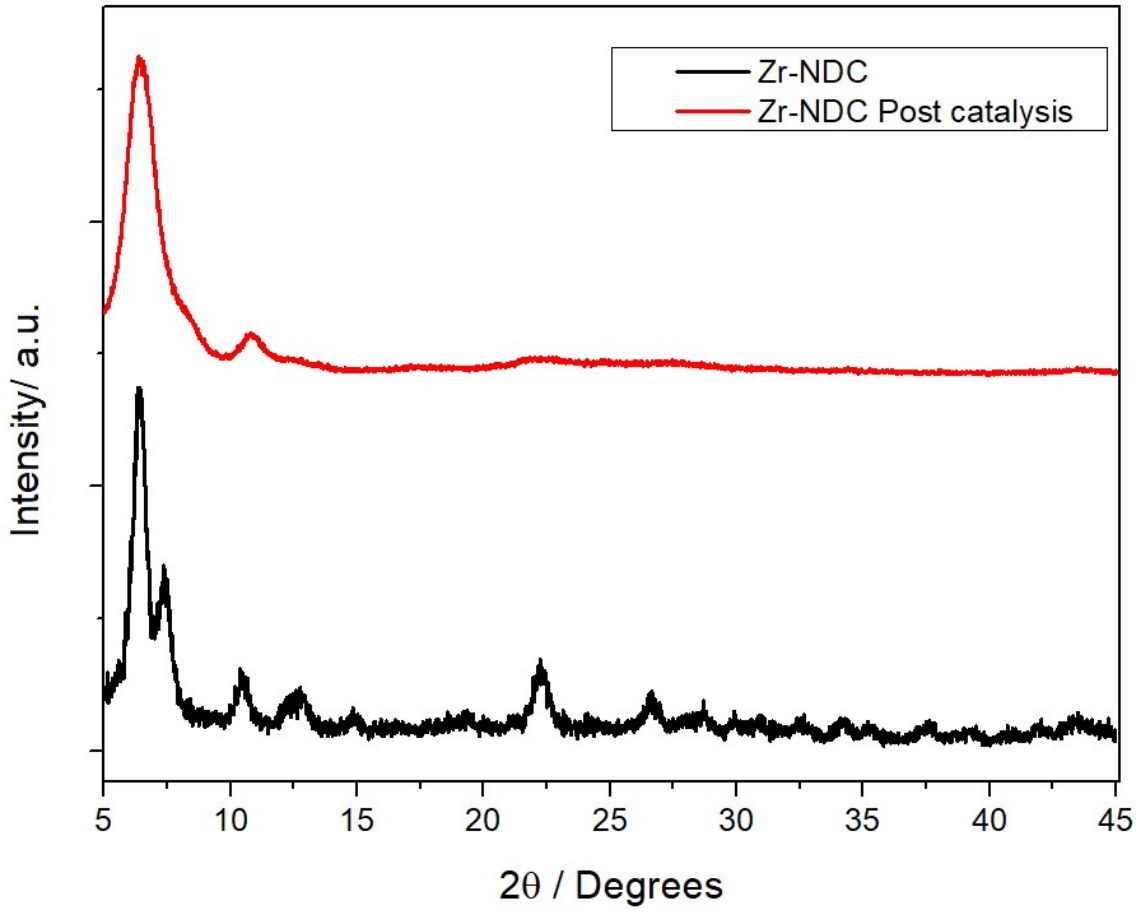

Figure S47: PXRD patterns of the ultra-small Zr-NDC MOF before and after the catalytic reaction.

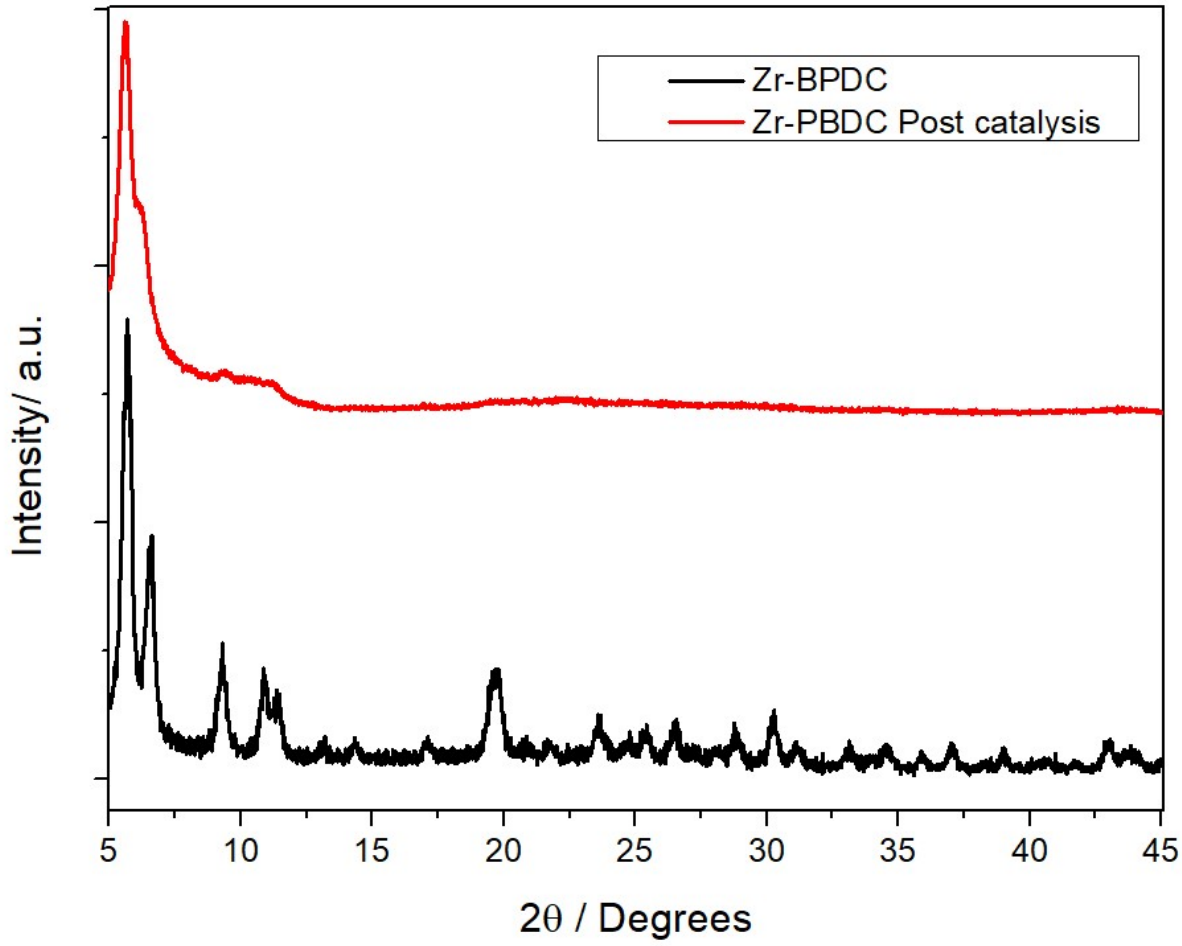

Figure S48: PXRD patterns of the ultra-small Zr-BPDC MOF before and after the catalytic reaction.

Comparison of Zr-BDC-NH_2 ultra-small nanoparticles with standard Zr-BDC-NH_2

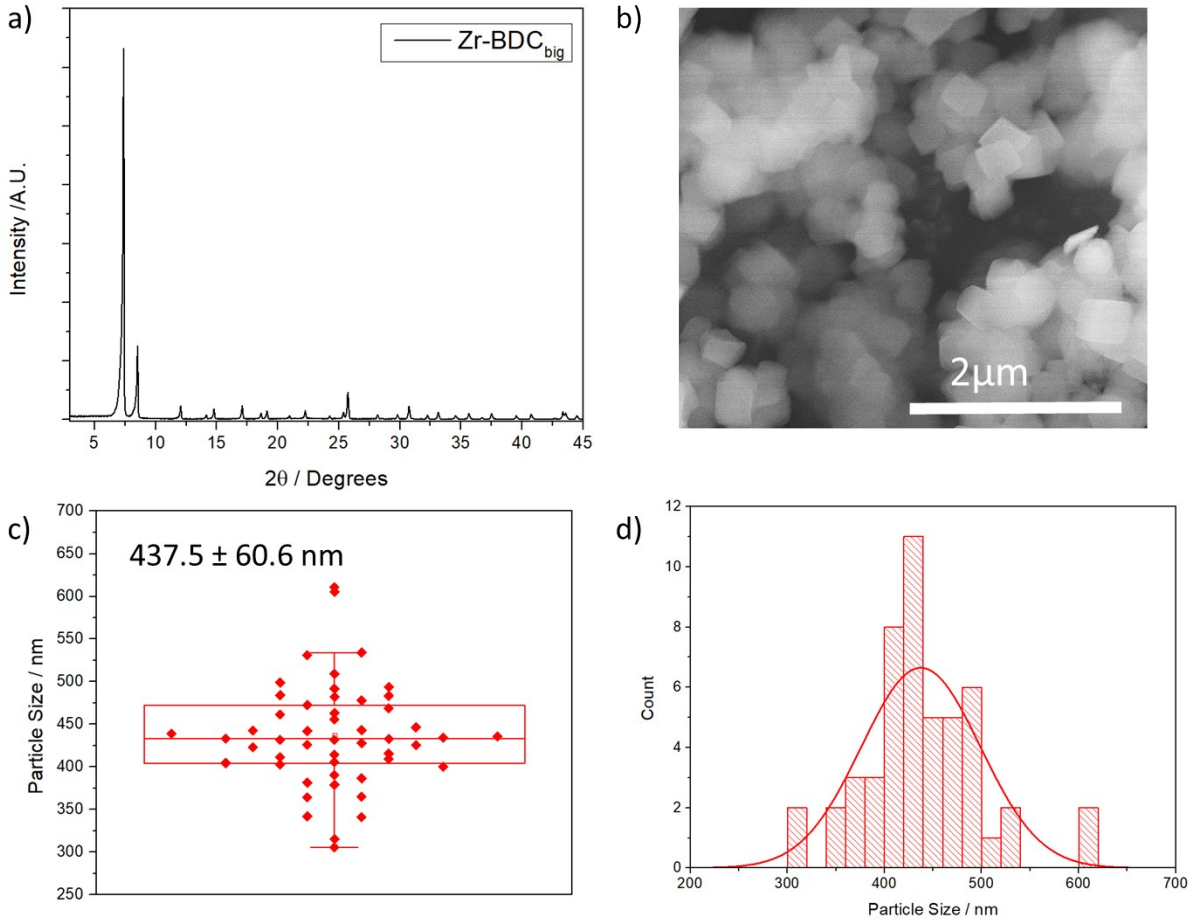

Figure S49: Characterisation of standard Zr-BDC-NH_2 of ca. 437.5 ± 60.6 nm. a) PXRD pattern, b) SEM image, c) box chart representation of particle sizes measured and d) histogram representation alongside distribution curve of the particle size.

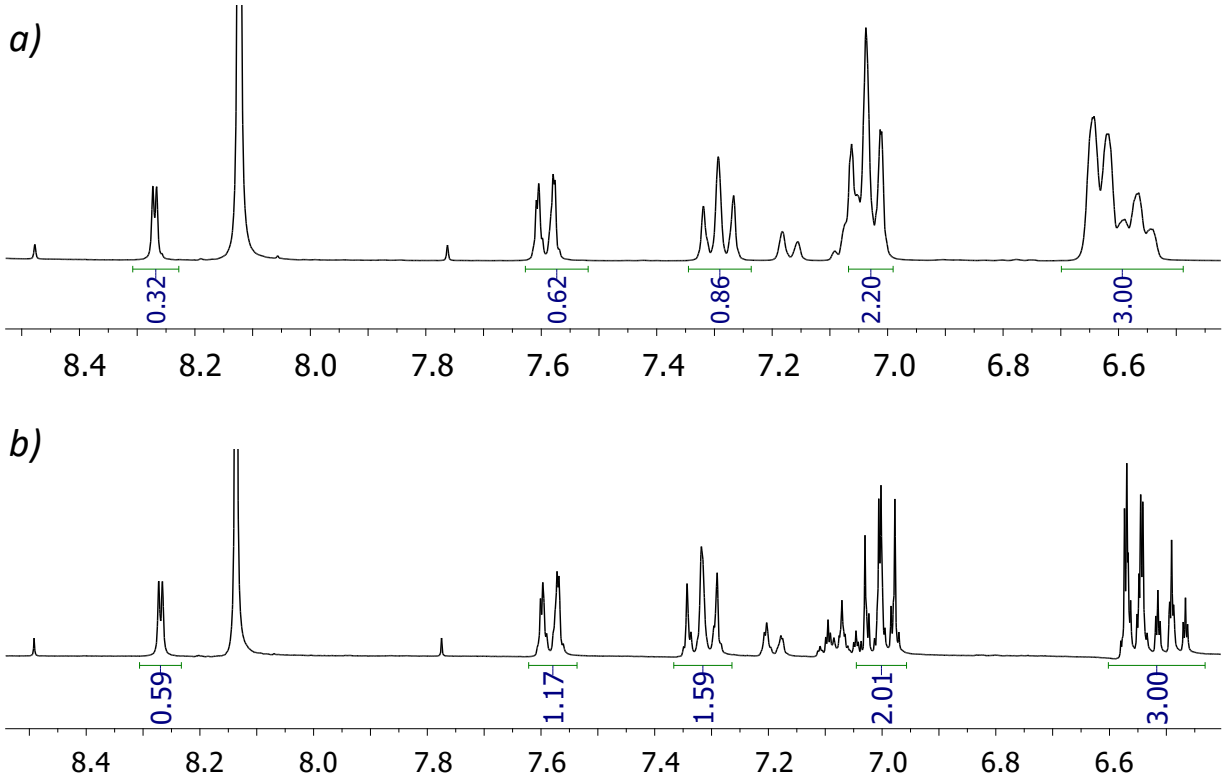

Figure S50. ^{1}H-NMR spectra (aromatic region) after 1 h of reaction between aniline and formic acid under solvent-free conditions in the presence of standard Zr-BDC-NH_2 (a) and ultra-small Zr-BDC-NH_2 nanoparticles (b). Reaction conditions: 5 eq. of acid, 10%wt. MOF, 35 ºC.

Table S9. Activity (reaction yield after 1 h, see Fig. S41) of Zr-BDC-NH_2 nanoparticles and standard Zr-BDC-NH_2 in the solvent-free formylation of aniline at 35ºC.

Particle size	**Yield/%**
Standard Zr-BDC-NH_2	22
Nanosized Zr-BDC-NH_2	34

Reaction between phenylacetic acid and benzylamine

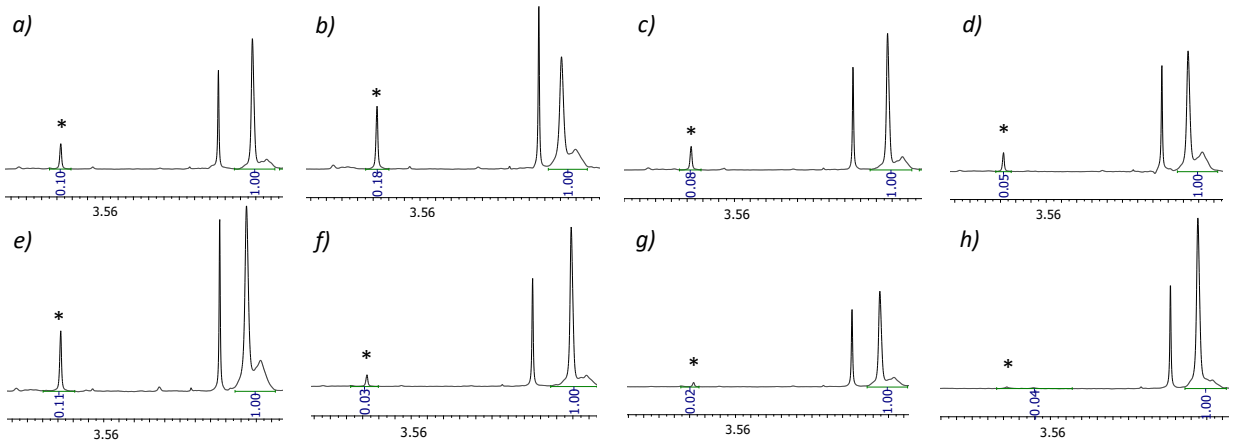

Figure S51. ^{1}H-NMR spectra (methylene region) of reaction between benzylamine and phenylacetic acid in the presence of Zr-BDC (a), Zr-BDC-NO_2 (b), Zr-BDC-NH_2 (c), Zr-BDC-OH (d), Zr -NDC (e), Zr-BPDC (f), $ZrOCl_2$ (g) and absence of MOF (h).

Table S10. Amidation of phenylacetic acid with benzylamine at 60ºC for 24 h in CD_3OD.

Composition	Yield/%	r_0/ µmol·h^{-1}
Zr-BDC	9	0.56
Zr-BDC-NO_2	15	0.94
Zr-BDC-NH_2	7	0.44
Zr-BDC-OH	5	0.31
Zr-NDC	10	0.62
Zr-BPDC	3	0.19
ZrOCl	2	0.13
Blank	4	0.25

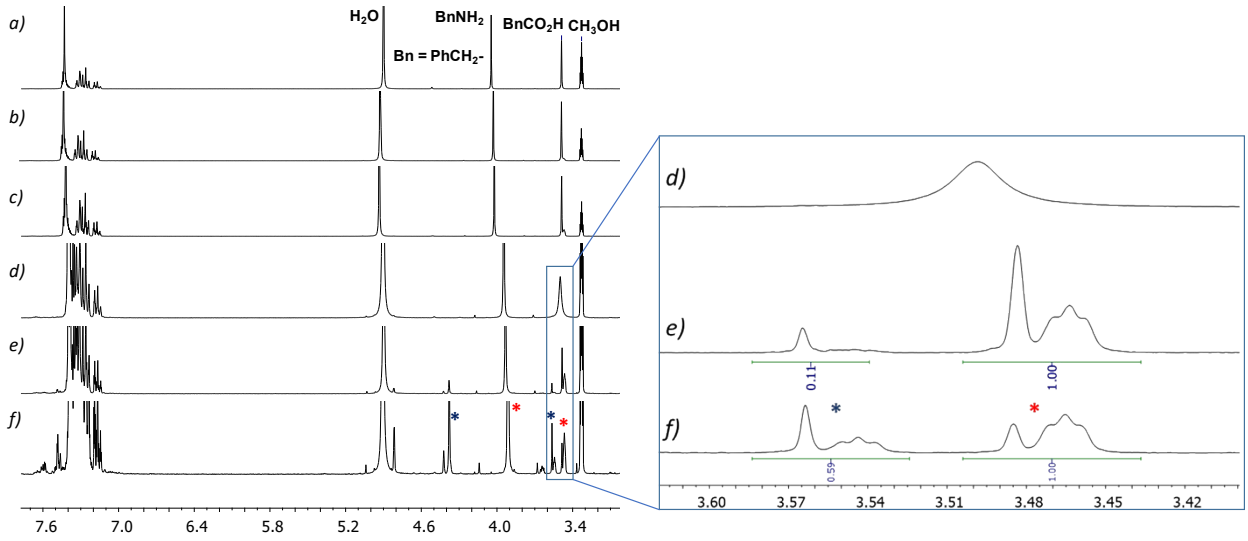

Figure S52. ^{1}H-NMR (300 MHz, CD_3OD) spectra (-CH_2- region of phenylacetic acid zoomed on the right part) after 1 h (a, d), 24 h (b, e), 72 h (c, f), of reaction between benzylamine (20 µL) and phenylacetic acid (20 mg) in CD_3OD at 60 ºC in absence (a, b, c) or presence of Zr-NDC (10 mg). Phenylacetic acid (pure) δ 7.30 (m, 5H, Ar-H), 3.61 (s, 2H, CH_2). Benzylamine (pure) δ 7.29 (m, 5H), 3.79 (s, 2H, CH_2). -CH_2- in the reaction media: *Phenylacetic acid (δ 3.48); *Benzylamine (δ 3.97); **N*-benzyl-2-phenylacetamide (δ 4.40, 3.55).

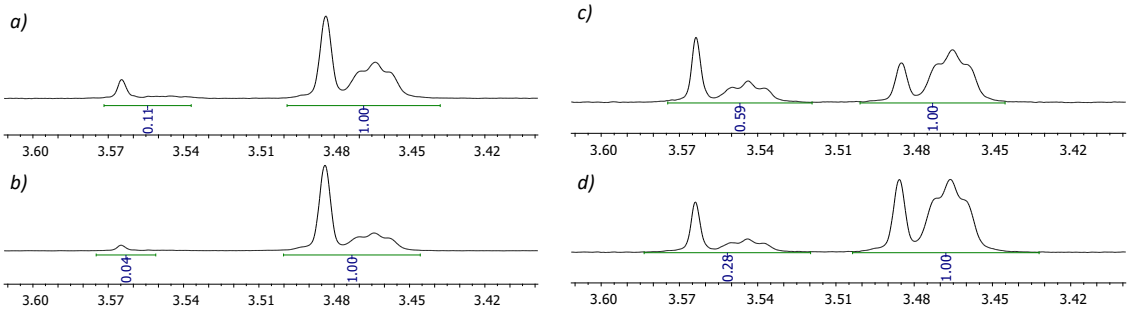

Figure S53. ^{1}H-NMR spectra (methylene region) after 24 h of the 1st (a) and 2nd (b) runs, and 72 h of the 1st (c) and 2nd (d) runs between benzylamine (20 µL) and phenylacetic acid (20 mg) in CD_3OD at 60 ºC in the presence of Zr-NDC (10 mg).

Table S11. Recyclability of Zr-NDC[a]

Run	Time/ h	Yield
1	24	9
	72	37
2	24	4
	72	22

[a] 10 mg MOF Zr-NDC, benzylamine (20 µL), phenylacetic acid (20 mg), CD_3OD (200µL) at 60 ºC.

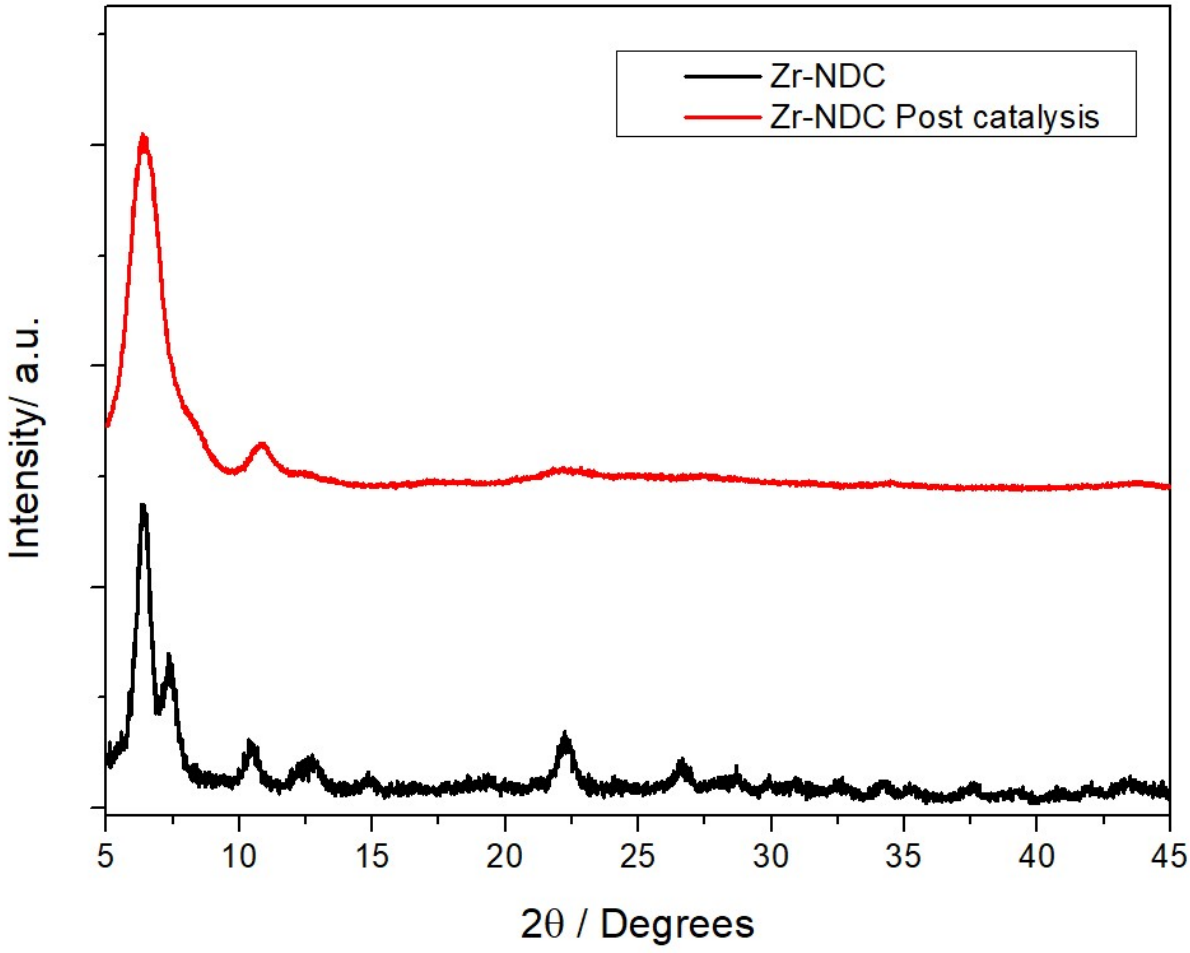

Figure S54: PXRD patterns of the ultra-small Zr-NDC MOF before and after the catalytic reaction between phenylacetic acid and benzylamine.

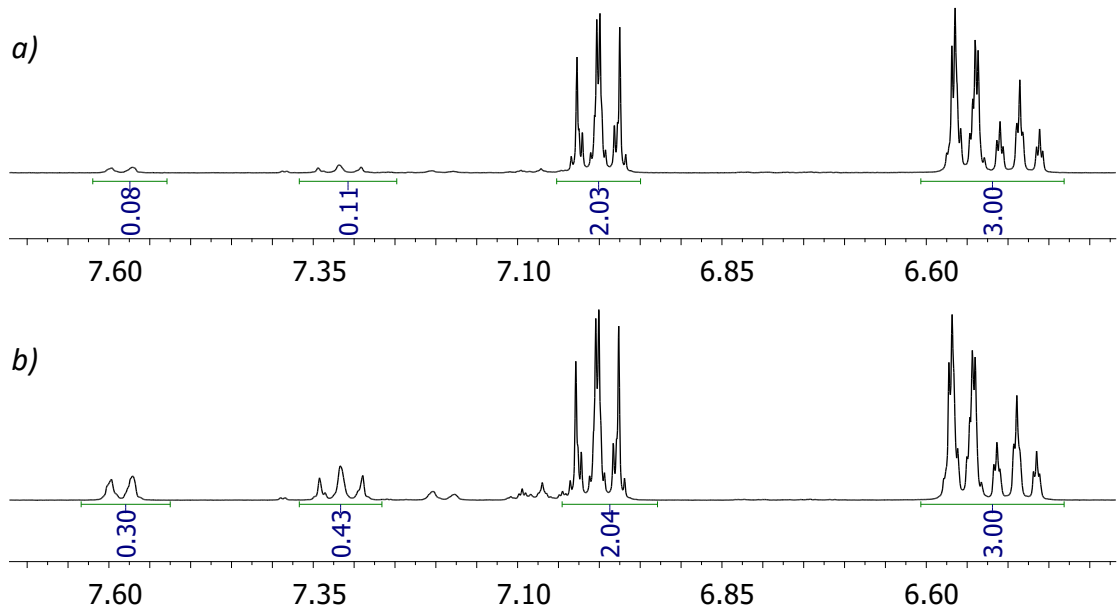

Figure S55. ^{1}H-NMR spectra (aromatic region) after 5 min (a) and 60 min (b) of reaction between aniline and formic acid in methanol-d as solvent in the presence of Zr-BDC-NH_2. Reaction conditions: 5 eq. of acid, 10%wt. MOF, 35 ºC.

Table S12. Kinetic study of the formylation of aniline (100 µL) with formic acid (200 µL) solvent-free or in methanol-d (100uL) at 35ºC in the presence of Zr-BDC-NH_2 (10 mg).

Time/h	Yield/%	
	CD_3OD as solvent	Solvent-free[a]
0.08	4	13
1	12	34

[a] From Tables S6 and S7

S.5. References

1 G. C. Shearer, S. Chavan, S. Bordiga, S. Svelle, U. Olsbye and K. P. Lillerud, *Chem. Mater.*, 2016, **28**, 3749–3761

2 I. A. Lázaro, *Eur. J. Inorg. Chem.* 2020, **2020**, 4284.